



Chinese Pharmaceutical Association
Institute of Materia Medica, Chinese Academy of Medical Sciences

Acta Pharmaceutica Sinica B

www.elsevier.com/locate/apsb
www.sciencedirect.com



ORIGINAL ARTICLE

Carbazole and tetrahydro-carboline derivatives as dopamine D₃ receptor antagonists with the multiple antipsychotic-like properties



Zhongtang Li^{a,†}, Fan Fang^{a,†}, Yiyan Li^{a,†}, Xuehui Lv^a, Ruqiu Zheng^a, Peili Jiao^a, Yuxi Wang^a, Guiwang Zhu^a, Zefang Jin^a, Xiangqing Xu^b, Yinli Qiu^b, Guisen Zhang^c, Zhongjun Li^a, Zhenming Liu^{a,*}, Liangren Zhang^{a,*}

^aState Key Laboratory of Natural and Biomimetic Drugs, School of Pharmaceutical Sciences, Peking University, Beijing 100191, China

^bJiangsu Nhwa Pharmaceutical Co., Ltd., Xuzhou 221116, China

^cJiangsu Key Laboratory of Marine Biological Resources and Environment, Jiangsu Key Laboratory of Marine Pharmaceutical Compound Screening, School of Pharmacy, Jiangsu Ocean University, Lianyungang 222005, China

Received 17 March 2023; received in revised form 28 June 2023; accepted 19 July 2023

KEY WORDS

Dopamine D₃ receptor;
Carbazole derivatives;
Tetrahydro-carboline;
Bitopic ligand;
Antipsychotic

Abstract Dopamine D₃ receptor (D₃R) is implicated in multiple psychotic symptoms. Increasing the D₃R selectivity over dopamine D₂ receptor (D₂R) would facilitate the antipsychotic treatments. Herein, novel carbazole and tetrahydro-carboline derivatives were reported as D₃R selective ligands. Through a structure-based virtual screen, ZLG-25 (D₃R K_i = 685 nmol/L; D₂R K_i > 10,000 nmol/L) was identified as a novel D₃R selective bitopic ligand with a carbazole scaffold. Scaffolds hopping led to the discovery of novel D₃R-selective analogs with tetrahydro-β-carboline or tetrahydro-γ-carboline core. Further functional studies showed that most derivatives acted as hD₃R-selective antagonists. Several lead compounds could dose-dependently inhibit the MK-801-induced hyperactivity. Additional investigation revealed that **23j** and **36b** could decrease the apomorphine-induced climbing without cataleptic reaction. Furthermore, **36b** demonstrated unusual antidepressant-like activity in the forced swimming tests and the tail suspension tests, and alleviated the MK-801-induced disruption of novel object recognition in mice. Additionally, preliminary studies confirmed the favorable PK/PD profiles, no weight gain and limited serum

*Corresponding authors.

E-mail addresses: zmliu@bjmu.edu.cn (Zhenming Liu), liangren@bjmu.edu.cn (Liangren Zhang).

[†]These authors made equal contributions to this work.

Peer review under the responsibility of Chinese Pharmaceutical Association and Institute of Materia Medica, Chinese Academy of Medical Sciences.

<https://doi.org/10.1016/j.apsb.2023.07.024>

2211-3835 © 2023 Chinese Pharmaceutical Association and Institute of Materia Medica, Chinese Academy of Medical Sciences. Production and hosting by Elsevier B.V. This is an open access article under the CC BY-NC-ND license (<http://creativecommons.org/licenses/by-nc-nd/4.0/>).

prolactin levels in mice. These results revealed that **36b** provided potential opportunities to new antipsychotic drugs with the multiple antipsychotic-like properties.

© 2023 Chinese Pharmaceutical Association and Institute of Materia Medica, Chinese Academy of Medical Sciences. Production and hosting by Elsevier B.V. This is an open access article under the CC BY-NC-ND license (<http://creativecommons.org/licenses/by-nc-nd/4.0/>).

1. Introduction

G protein-coupled receptors (GPCRs) are the most prominent family of membrane proteins and are comprised of more than 800 members, of which the majority are implicated in the pathophysiology of neurodegenerative disorders^{1–3}. Dopamine receptors belong to the class A GPCR family and mediate the physiological functions of dopamine, a neurotransmitter and hormone with a catecholamine structure. Based on the coupling to either $G_{\alpha_{s/olf}}$ proteins, or $G_{\alpha_{i/o}}$ proteins to stimulate or inhibit the production of the second messenger cAMP, respectively, dopamine receptors are categorized into two subfamilies: D₁-like (D₁R and D₅R) and D₂-like (D₂R, D₃R, and D₄R)⁴. D₃R belongs to the same D₂-like receptor family as D₂R, sharing a high level of homology with them. Since it was cloned and characterized, the D₃R has been a target of therapeutic interest due to its relatively localized expression within mesolimbic neurocircuitry, including the nucleus accumbens, islands of Calleja, and ventral striatum^{5–7}. The polymorphism of ser9gly in the first exon of D₃R gene is associated with schizophrenia⁸. The level of D₃R in the striatum increases in patients with schizophrenia and decreases with those treated with antipsychotic drugs⁹.

A number of studies employed a strategy for schizophrenia drug development that avoided EPS elicited with many antipsychotics is targeting D₃R and avoiding the D₂R effects¹⁰. As shown in Supporting Information Table S1, the diverse bitopic ligands with highly D₃R-selectivity had been explored to develop novel D₃R compounds with clinical ambitions, exploiting unique interactions at the D₃R binding pocket^{11–22}. Novel therapeutic applications of these known molecules with D₃R-selectivity have been disclosed, which encouraged the continuous discovery of novel series of D₃R selective ligands²³. D₃R-selective ligands in clinic and clinical trials were shown in Fig. 1A. S33138 was a preferential dopamine D₃ versus D₂ receptor antagonists identified preserving, enhancing cognitive function and increasing front cortical cholinergic transmission^{24,25}. ABT-925 is a selective D₃R antagonist with an approximately 100-fold higher *in vitro* affinity for dopamine D₃ versus D₂ receptors, which had been examined in a phase I trial for acute exacerbation of schizophrenia but ABT-925 failed in a phase II. The reason of the failure might be the insufficient occupancy to D₃ receptors at the doses used in this trial^{26,27}. GSK598809, a D₃R antagonist with >100-fold selectivity for D₃ > D₂ receptors, belonged to a novel series of 1,2,4-triazol-3-yl-azabicyclo[3.1.0]hexanes with high affinity and selectivity for the D₃ receptor and excellent pharmacokinetic profiles^{28,29}. The treatment of substance addiction by GSK598809 had been examined in obese individuals and severe chronic smokers (*i.e.*, NCT1039454 and NCT01188967 on ClinicalTrials.gov). However, the potential cardiovascular liability

of GSK598809 at high doses increased the hurdle of clinical trials³⁰. Buspirone was developed as a D₃-preferring 5HT_{1A} antagonist studied in alcoholics and found to reduce anxiety, in particular during withdrawal (*i.e.*, NCT00360191 and NCT00875836 on [clinicaltrials.gov](http://ClinicalTrials.gov)). Interestingly, selective D₃R engagement of buspirone was only observed after oral dosing, while intramuscular administration was engaging also the D₂R, indicating buspirone metabolites generate by the first passage through the liver could be the actual active moiety³¹. RGH188 (cariprazine, CRP) was characterized as a D₃R preferential binding ligand with a 10-fold D₃R/D₂R selectivity. Notably, CRP exerted a cognitive-enhancing effect in the *in vivo* tests, which was thought to be related to its high affinity and preference for D₃ versus D₂ receptor³². F17464 was discovered as a unique >80-fold D₃ over D₂ receptor preferential antagonist, which has been demonstrated selective D₃ receptor occupancy in a human positron emission tomography (PET) imaging study³³. In a phase II schizophrenia acute exacerbation study, clinical antipsychotic efficacy with no weight gain, no extrapyramidal disorder observed³⁴. Furthermore, F17464 could rescue valproate induced impairment in a rat social interaction model of autism, probably by increasing dopamine release in the prefrontal cortex and lateral forebrain–dorsal striatum³⁵. Although no highly selective D₃ ligands have been approved by US Food and Drug Administration (FDA), selective D₃ ligands have demonstrated many advantages in clinical trials for mood regulation, cognitive protection, and low side effects.

However, the development of selective D₃R ligands has been challenging due to the high sequence identity and homology. The D₂R and D₃R share 74% identity between their transmembrane domains (TMs) and 94% identity between their putative orthosteric binding sites (OBS), where the endogenous agonist dopamine binds³⁶. To improve selectivity, most D₃R ligands that share several well-known scaffolds with a primary pharmacophore, bind to the OBS and a secondary pharmacophore binding to the second binding pocket (SBP) or an allosteric binding site (ABS)³⁷. GPCR ligands with such a scaffold have been depicted as bitopic binders, which can benefit high subtype affinity and selectivity^{38,39}. In this study, we report the discovery of a novel series of D₃R selective antagonists with desirable antipsychotic potency *in vivo*. From the initial hit compounds containing the carbazole scaffold, over 60 bitopic structural analogs were synthesized and evaluated for a comprehensive investigation of structure–activity relationships (SAR), which led to the identification of compound **36b** as a potent and blood brain barrier (BBB) penetrable D₃R selective antagonists suitable for *in vivo* characterization. Furthermore, compound **36b** exhibited potential antipsychotic activities *in vivo* with moderate safety profiles in psychotic side effects and hERG channel inhibition. *In vivo*,

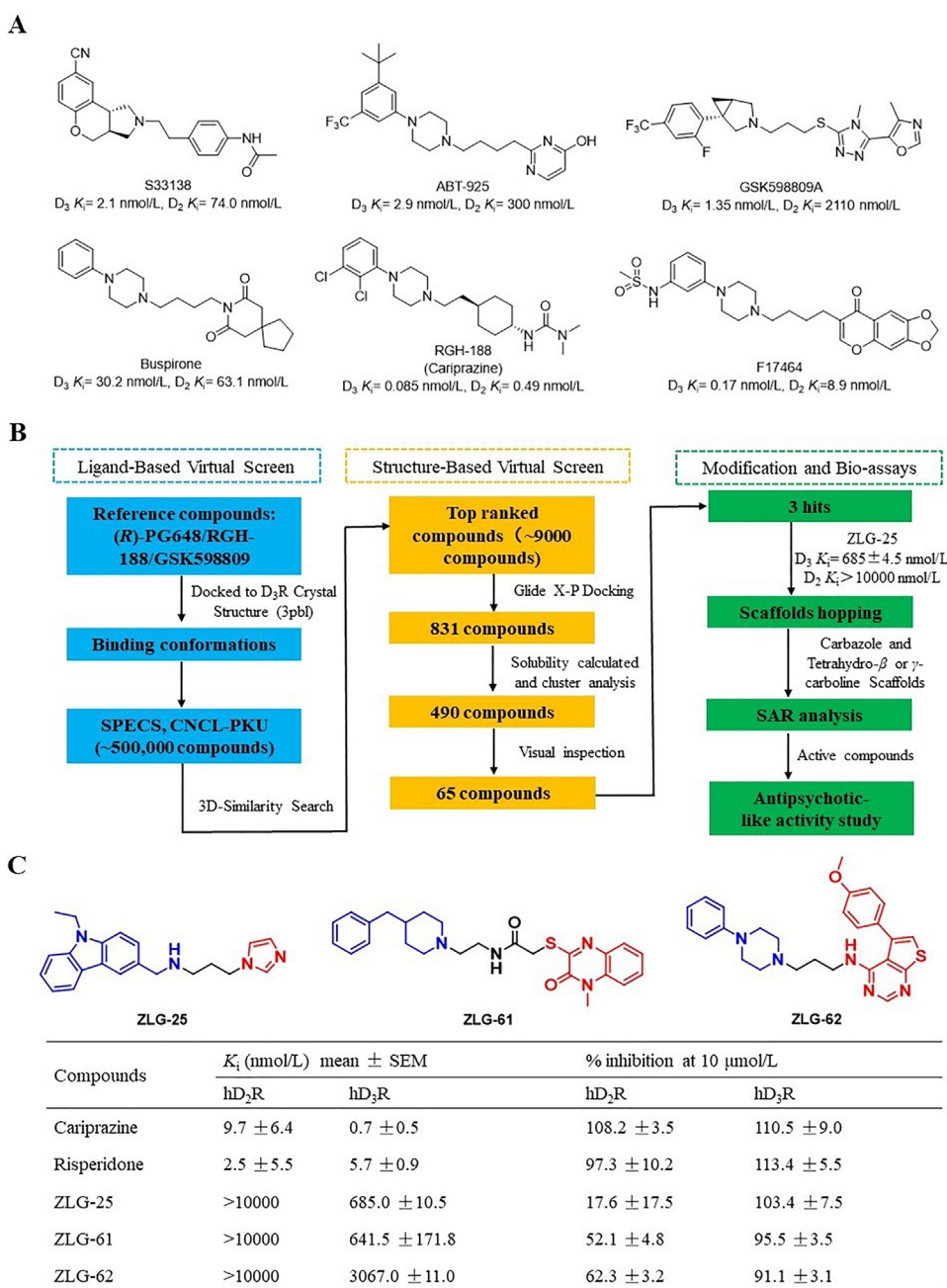


Figure 1 (A) D₃R-selective ligands in clinic and clinical trials. (B) General workflow of D₃R ligands identification. (C) Chemical structures of 3 identified hits and the binding affinities.

pharmacokinetics (PK) profiles and exquisite target selectivity of compound **36b** were also satisfactory. Taken together, compound **36b** was characterized as an excellent lead compound for further optimizations of the novel D₃R selective antagonists with distinct antipsychotic-like effects *in vivo*.

2. Results and discussion

2.1. Structure-based virtual screening

Our workflow of virtual screening is summarized in the protocol in Fig. 1B. A 3D shape-based similarity screening connected docking-based virtual screening approach was used in our

study^{40–42}. Three compounds with high affinity and selectivity for the D₃R (R)-PG468, RGH-188, and GSK598809A were selected as the benchmark compounds for their representative secondary pharmacophore structures, which were to benefit high subtype selectivity. After preparing the co-crystal structure (PDB ID: 3pbl, Supporting Information Table S2) well, these three compounds were docked into the D₃R using the induced-docking module of Maestro obtaining three binding conformations for each compound (Supporting Information Fig. S1). Aiming to seek more potent ligands, 3D shape-based similarity virtual screening approaches were employed to search more than 600,000 compounds from the SPECS chemical library, the ChemDiv chemical library, and the Chinese National Compound Library of Peking University

(PKU-CNCL) databases by ROCS 3.1.2 (OpenEye Scientific Software, Inc.) program. As a result, the top 3000 compounds were retained based on the 'Shape Tanimoto' score. Next, the Glide molecular docking module was used to screen the selected compounds from the 3D-similarity search, which were sorted by docking score, and all compounds within the top one percent were obtained. Because the residue Asp110 was essential for the binding affinity, compounds forming the ionic interaction with Asp110 were isolated using the PoseFilter module in the Maestro platform. Based on compound docking results and physicochemical properties, 65 compounds were purchased for further biological activity tests (Supporting Information Fig. S2). All active compounds passed the pan assay interference compounds (PAINS) test by PAINS-remover⁴³.

For the primary screen, a single high concentration (10 $\mu\text{mol/L}$) of test compound was tested by radioligand binding assays on the CHO cells stably expressing hD₂R and hD₃R (Table S2), and those compounds that exhibited >75% inhibition were rescreened in full concentration-response format to estimate their affinity (K_i) values. Risperidone (RPD) and CRP were used as the positive drugs. From the 65 selected compounds, ZLG-25, ZLG-61, and ZLG-62 showed >90% inhibition for the D₃R at 10 $\mu\text{mol/L}$ (Table S3). Further tests accessed the affinity values of ZLG-25 ($K_i = 685 \pm 4.5 \text{ nmol/L}$), ZLG-61 ($K_i = 641.5 \pm 171.8 \text{ nmol/L}$), and ZLG-62 ($K_i = 3067.0 \pm 11.0 \text{ nmol/L}$) for D₃R (Fig. 1C). Then, the D₂R K_i of these compounds were also tested and found to be 10–20 fold higher than that to D₃R. Moreover, representative molecular properties of all the tested compounds were predicted by the Maestro 11.5 *Qikprop* module. The CNS drug-like properties of the selected compounds were identified as favorable values defined as a $\log P < 3$, polar surface area (PSA) < 90 \AA^2 , and BBB permeability with the ADMET_BBB_Level < 3⁴⁴. Among the selected compounds, ZLG-25 showed a superior selectivity, which provided a potential starting scaffold for structural optimization to improve biological activities and physicochemical properties (Supporting Information Table S4).

2.2. Molecular modeling of ZLG-25 and design of bitopic ligands

To explore the binding properties of ZLG-25 at D₃R, the induced-fit docking (Fig. 2A–B) and molecular dynamic (MD) simulation (Supporting Information Fig. S3) were performed in Schrodinger 2018.1. The results of MD were well consistent with the docking results, depicting a bitopic binding mode. The carbazole moiety of ZLG-25 was found located at the OBS forming π - π interactions with Phe345 and Phe346. The protonated nitrogen atom in the linker chain formed a salt bridge with the carboxylate of Asp110 offering a key and strong interaction. The imidazole moiety was oriented toward the SBP constructed by extracellular loop1, loop2, helices I, helices II and VII, forming the ionic interaction with Glu90. Based on the scaffold of ZLG-25, a series of more typical bitopic molecules were expected to be obtained as D₃R selective ligands by attaching a D₃R-preferring SBP binding motif to the amine group (Fig. 2C). The carboxamide replaced the SBP binding moiety-linked aromatic group, which was thought to occupy more space in the SBP and provide more interactions than the imidazole moiety. The scaffold hopping or structural simplification strategy was further used to improve the rigid carbazole structure by moving the nitrogen atom in the linker chain to the ring B of the carbazole moiety⁴⁵. In 'hopping I', the secondary amine was converted to the tertiary amine at position 4, obtaining

the tetrahydro- β -carboline scaffold. Furthermore, 'hopping II' was processed by moving the tertiary amine to position 3 to obtain the tetrahydro- γ -carboline scaffold by (Fig. 2C). Therefore, started from ZLG-25, a series of carbazole and tetrahydro-carboline derivatives were designed to discover novel D₃R-selective ligands.

2.3. Chemistry

In Scheme 1A, carbazoles with different alkyl (methyl, ethyl, and isopropyl) groups were used as the starting materials. The formyl group at position 4 was incorporated in the solution of DMF and POCl₃ in 80%–95% yield. The subsequent incorporation of the linker moiety was achieved by the reductive amination reaction affording derivatives **3a–c**, with adding NaBH(OAc)₃ for multiple times. However, benzaldehyde **7** was not obtained with the same procedures as **2a–c**, but rather through Fisher indole synthesis reaction and oxidative dehydrogenation in one pot, obtaining intermediate **6** (Scheme 1B). It was found that if the reaction was carried out in the absence of acid environment in 100 °C, the phenyl hydrazine must be with hydrochloride for the formation of NH₄Cl. The aromatization by oxidation sequentially happened in one pot under O₂. Intermediates **6** were oxidized to an aldehyde group offering intermediates **7**. Derivatives **8** was obtained by a similar fashion as **3a–c**.

As shown in Scheme 1C, the cyclohexanone (**4**) and the methyl 4-hydrazineylbenzoate (**9**) was refluxed in AcOH to synthesize the intermediate **10** in high yield. Another two steps were proceeded for converting methyl formate intermediate to a formyl intermediate **12**. A similar process was performed to obtain derivatives **13**. To further understand the importance and effect of the SBP binding moiety; derivatives **17a–f** were synthesized by replacement of the imidazole moiety with various aromatic rings (Scheme 1D). Compound **2b** was reacted with the 3-aminopropanol or 4-amino-1-butanol and reduced to obtain intermediates **14a/b**. The secondary amines were sequentially protected with the Boc group, and sulfonated with benzenesulfonyl group affording intermediates **16a/b**. Subsequent substitution reactions and *N*-Boc deprotection resulted into the desired products **17a–f**.

The derivatives **22a–c** were accessed through a three-step synthesis outlined in Scheme 2A. The *tert*-butyl (3-aminopropyl) carbamate (**18**) was used to prepare intermediates **20a** in the cooperation with dimethylcarbamic chloride and dimethylsulfamoyl chloride. Compounds **20b/c** were obtained through the amide coupling in the presence of EDCI and DMAP, followed by the reductive amination to furnish the final products **22b/c**. Additionally, a longer chain linker moiety was explored with the starting material **19** through the same three-step synthesis route to afford the desired final derivatives **23a–m** (Scheme 2A). A cyclohexyl ring as linker was also investigated. As detailed in Scheme 2B, *tert*-butyl ((1*R*,4*R*)-4-aminocyclohexyl) carbamate (**24**) and 1*H*-indole-2-carboxylic acid (**25**) were utilized to prepare the intermediate **26** and resulted in the final compound **27** through a similar two-step, one-pot synthesis methods. Two intermediates, **28a/b**, were obtained to synthesize the **29a/b** with *tert*-butyl (4-bromobutyl) carbamate in potassium carbonate. Treatment of **29a/b** with TFA afforded amine **30a/b**. To furnish the desired targets **31a–e** in high yield, the amide coupling catalyzed by EDCI and DMAP was used (Scheme 2C).

Tetrahydro- γ -carboline derivatives **36a–k** were prepared as mentioned in Scheme 3A, from the starting materials

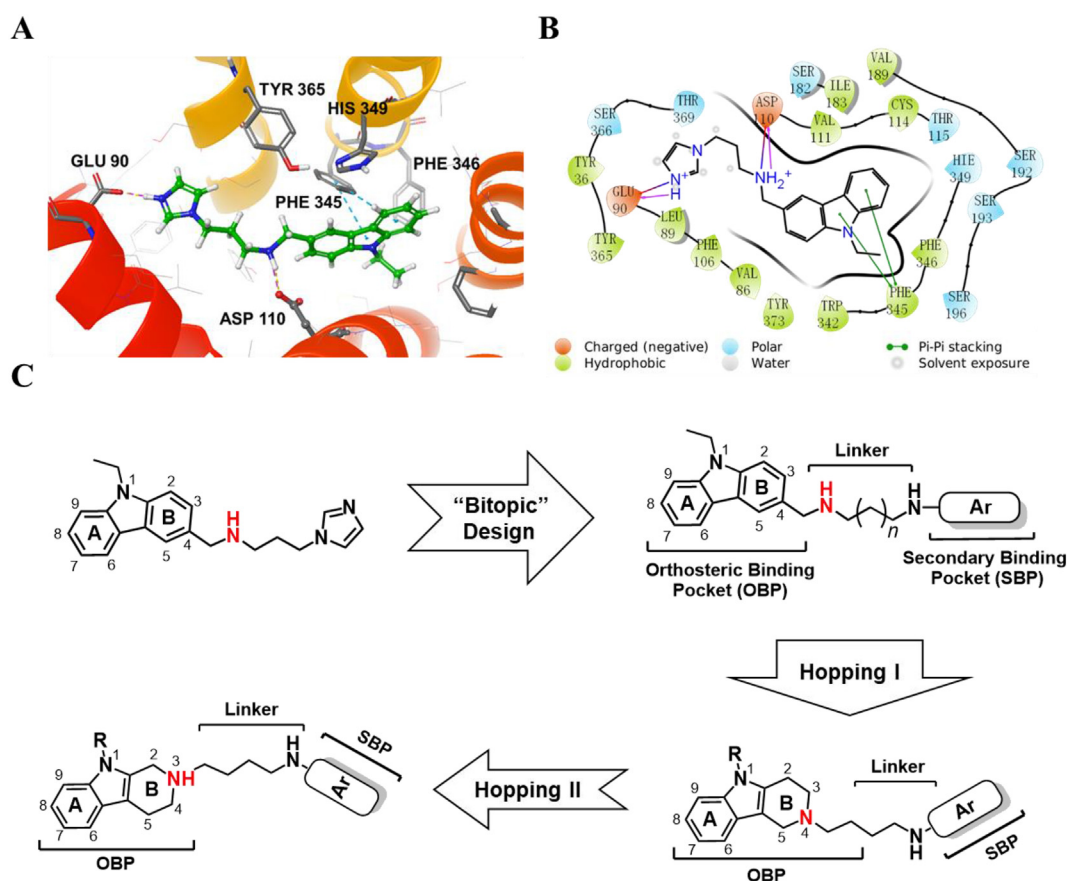


Figure 2 Protein–ligand contacts histogram ZLG-25 (A) and corresponding 2D diagram (B); The structure design strategy in this work (C).

phenylhydrazine **32a/b** and piperidine-4-one. Compounds **34a/b** served as the critical intermediates for synthesizing compounds, of which the synthetic protocol was the same as the intermediate **10**. Intermediates **35a/b** were prepared with commercially available *tert*-butyl (4-bromobutyl)carbamate. Then, compounds **35a/b** on treatment with CF₃COOH in CH₂Cl₂ afforded the primary amine intermediates to obtain the target compounds **36a–k** by the same amide coupling reaction. Tetrahydro- β -carboline derivatives **42a–f** were synthesized from the starting materials 2,3,4,9-tetrahydro-1*H*-pyrido[3,4-*b*]indole (**37**) (Scheme 3B). The NH at piperidyl structure was selectively protected by the Boc group and then the NH at indole structure was alkylated by CH₃I or CH₃CH₂I to offer intermediates **39a/b**. After the secondary amine intermediates **40a/b** afforded on treatment with CF₃COOH in CH₂Cl₂, compounds **41a/b** was obtained by the reaction with *tert*-butyl (4-bromobutyl)carbamate. Final compounds **42a–f** were prepared by the same process as **36a–k**.

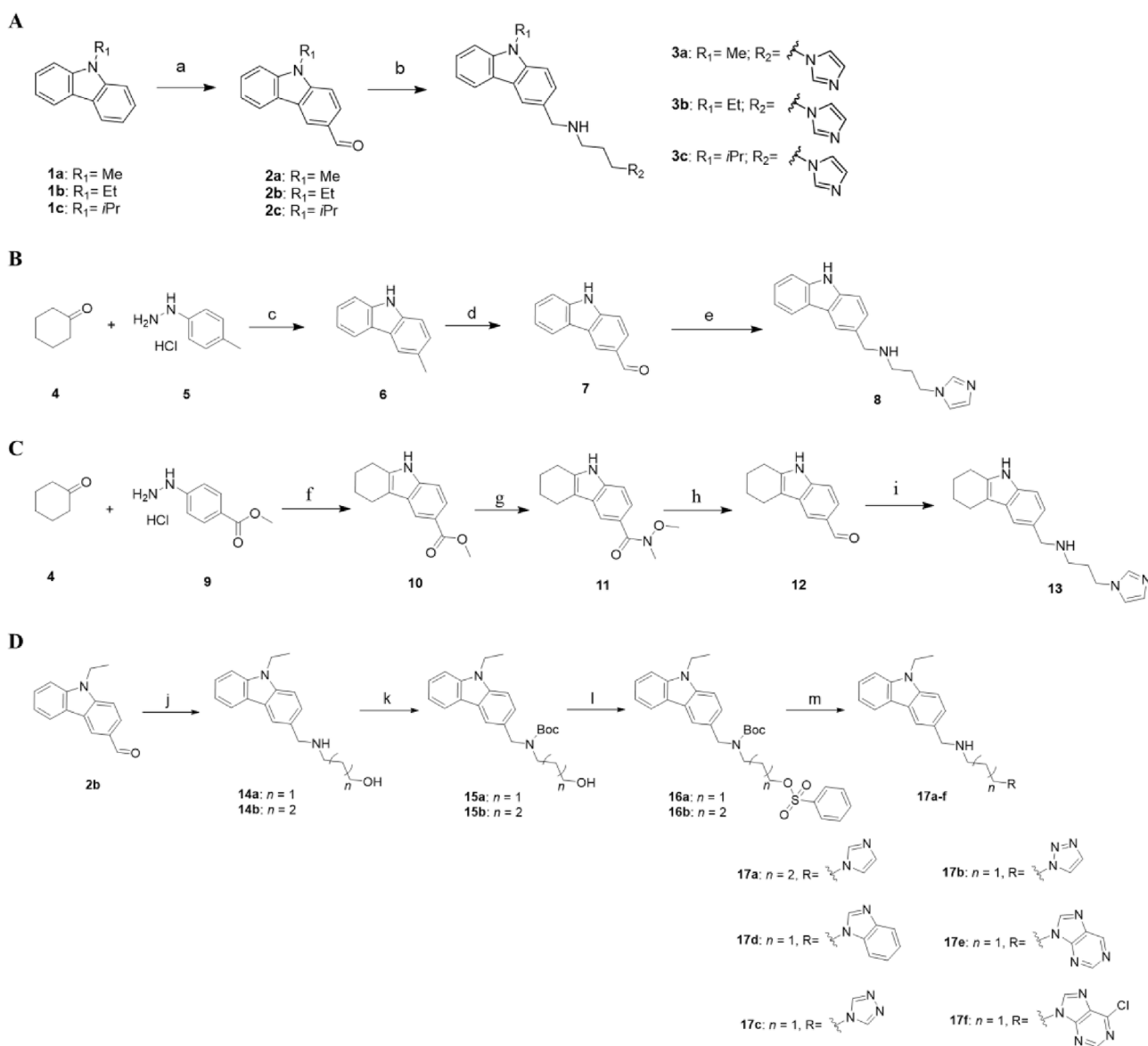
2.4. Structure–activity relationships study

To increase the binding affinity of hit compound ZLG-25 at the D₃R, the SAR study and scaffold hopping of the carbazole scaffold were investigated. More than 60 derivatives were synthesized and the binding affinities and selectivity profiles at D₂R and D₃R were identified. To explore the key role of carbazole moiety in a high selectivity for D₃R over D₂R, different alkyl substitutions on the 1-position nitrogen of the carbazole moiety and the impact of aromaticity on the carbazole nucleus were first examined. The

linker and imidazole moiety were then replaced with other entities to increase the binding affinity at D₃R as described above.

Radioligand competition binding assays were performed by measuring the ligands' ability to compete with [³H] spiperone for the CHO cells stably expressing hD₂R and hD₃R^{9,39,46–49}. The results are expressed as the inhibition values at 10 μ mol/L for all the derivatives presented in Tables 1–5. The K_i values were tested for any compound with an inhibition above 75% for D₂R or D₃R. Following the discovery of novel structures with high selectivity for D₃R, a structural analysis to understand the basis for this was initiated from the modification of carbazole moiety. As shown in Table 1, the alkylation at the N position of carbazole was explored, and the comparison of affinities to D₃R showed that ethyl (**3b**) and isopropyl (**3c**) groups had improved potency compared to the methyl group (**3c**) and hydrogen (**8**). The binding mode of ZLG-25 (**3b**) displayed strong π – π interactions between the carbazole and the aromatic residues (Phe345/Phe346/His349). To verify the importance of aromaticity, 2,3,4,9-tetrahydro-1*H*-carbazole was introduced to the analogs (**13**), which suggested the decreased potency as expected. The linker chain composed of four carbon atoms (**17a**) showed comparative potency with ZLG-25 (Table 1). Subsequently, a survey of heterocyclic replacements for the imidazole moiety was performed, such as 1,2,3-triazole (**17b**), 1,3,4-triazole (**17c**), benzimidazole (**17d**), purine (**17e**) and 6-Cl-purine (**17f**), among which only **17b** exhibited an improved binding affinity compared to ZLG-25.

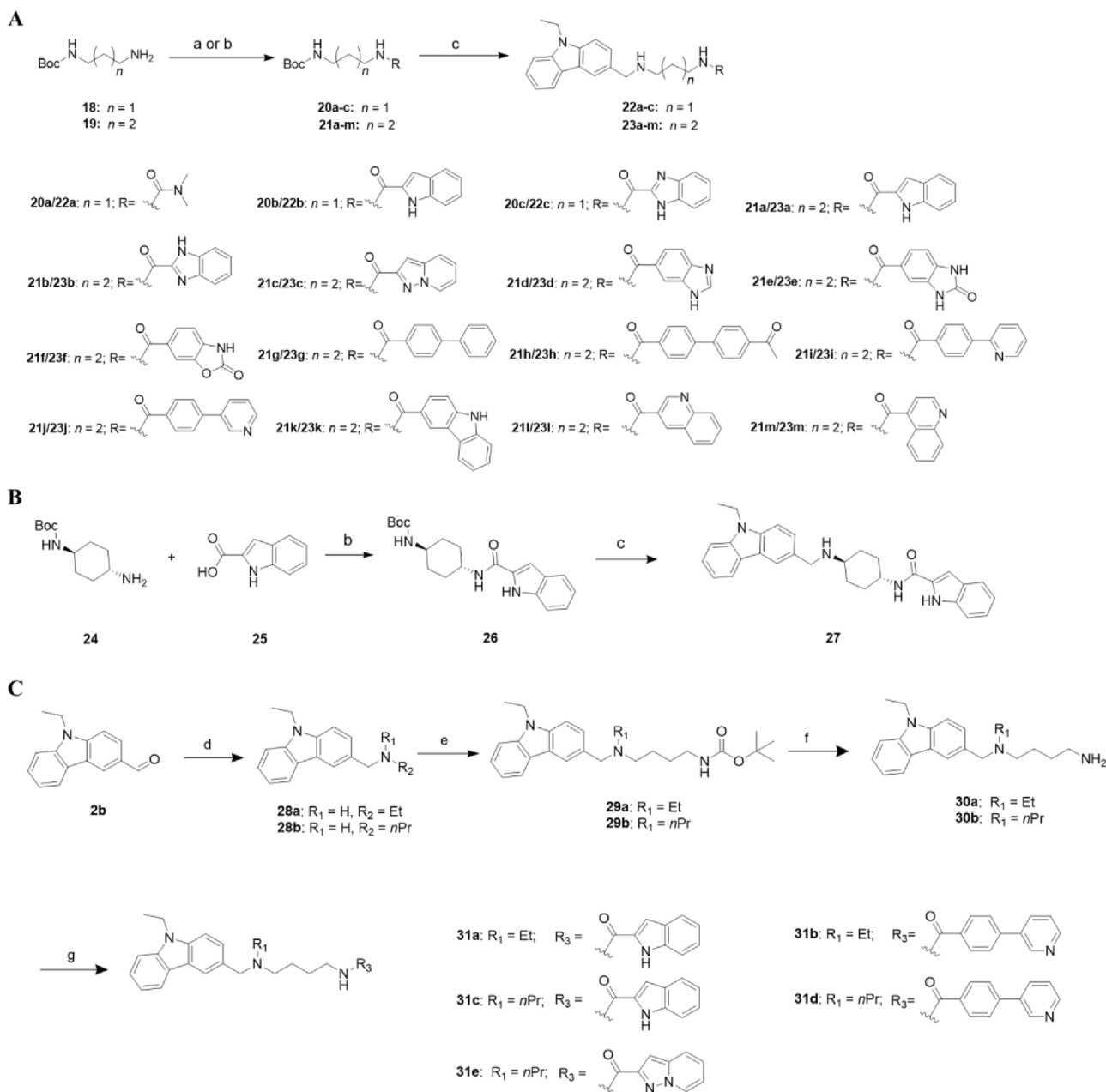
As shown in Table 2, when the linker length was kept at three-carbon units, the replacement of the imidazole group by



Scheme 1 Synthesis of 9-ethyl-9H-carbazole derivatives. Reagents and conditions: (a) DMF, POCl₃, 130 °C; (b) 3-(1H-imidazole-1-yl)propan-1-amine for **3a–c**, MeOH. (c) O₂ (1 atm), DMSO, 100 °C; (d) DDQ, MeOH/H₂O, r.t.; (e) 3-(1H-imidazole-1-yl)propan-1-amine, NaBH(OAc)₃, MeOH. (f) AcOH, TsOH, reflux; (g) 1) NaOH, MeOH/H₂O, r.t.; 2) *N,N*-Dimethylhydroxylamine hydrochloride, EDCI, DMAP, CH₂Cl₂; (h) LiAlH₄, THF, 0 °C; (i) 3-(1H-imidazole-1-yl)propan-1-amine for **13**, NaBH(OAc)₃, MeOH. (j) 3-Aminopropanol or 4-amino-1-butanol, MeOH/NaBH(OAc)₃, r.t.; (k) (Boc)₂O, CH₂Cl₂, r.t.; (l) Benzenesulfonyl chloride, DMAP, 0 °C, 5 h; (m) 1) 1H-*N*-Heterocycle, NaH, TBAL, DMF, –5 °C; 2) CF₃COOH, CH₂Cl₂, r.t.

dimethylurea (**22a**) failed to give improved binding profiles. And, the aromatic carboxamide moieties (**22b/c**) were also explored but were found to be less potent versus ZLG-25. When the propyl linker was replaced with a butyl (**23a**) and cyclohexyl (**27**) linker, both compounds showed a significant improvement in D₃R binding affinity ($K_i = 62.6$ nmol/L for **23a** and $K_i = 52.1$ nmol/L for **27**). Intending to improve the D₃R binding affinity, we realized that the butyl linker would likely be suitable to explore the second binding region of bitopic compounds. Next, we investigated the replacement of the indole-2-carboxamide moiety of **23a** with different aromatic carboxamide moieties (**23b–m**) to fit the SBP. Comparing with compound **23a**, 1H-benzo[*d*]imidazole (**23b/23d**) exhibited decreased binding affinity at D₃R ($K_i = 577.6$ nmol/L/

$K_i = 125.1$ nmol/L). The pyrazolo[1,5-*a*]pyridine (**23c**) showed a comparable D₃R binding affinity ($K_i = 45.7$ nmol/L) to **23a**. Moreover, 1,3-dihydro-2H-benzo[*d*]imidazole-2-one (**23e**) and benzo[*d*]oxazol-2(3H)-one (**23f**) were both used as they have been reported in numerous D₃R selective compounds, showing the K_i values of 99.3 and 95.1 nmol/L, respectively. Further replacements with larger moieties were also explored such as the 1,1'-biphenyl-4-carboxamide moiety (**23g**) which led to a decreased D₃R affinity while 4'-acetyl-[1,1'-biphenyl]-4-carboxamide moiety (**23h**) and showed an increased D₃R affinity ($K_i = 24.2$ nmol/L). When the substituent groups on the *para*-position of benzamide were converted into pyridyl groups (**23i/j**), the binding affinity was found to have an approximately 10-fold improvement for D₃R versus the



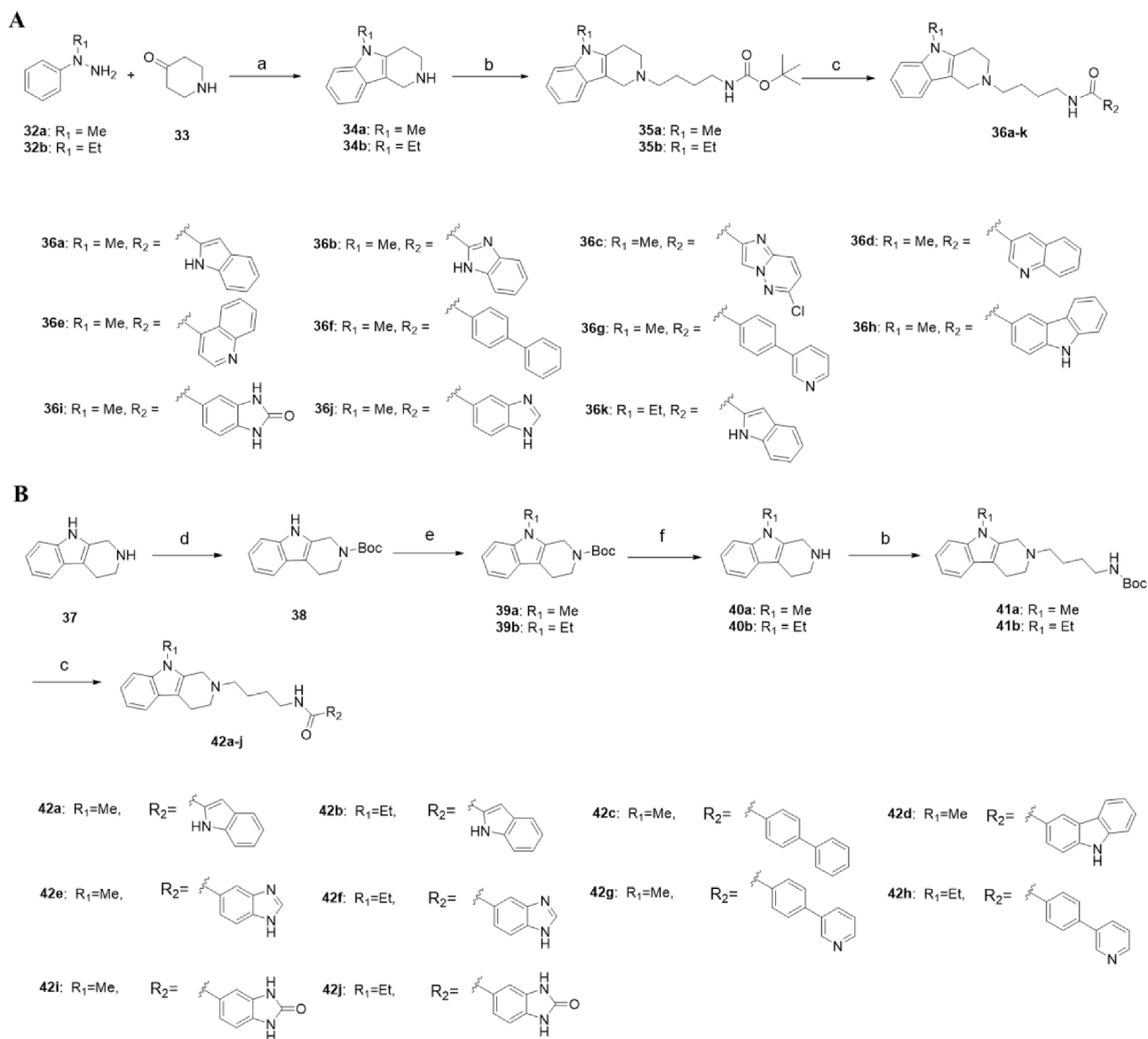
Scheme 2 Synthesis of carboline derivatives. Reagents and conditions: (a) for **20a**, dimethylcarbamic chloride, NaH, DMF; (b) for **20b/c** and **21a–m**, aryl formic acid, EDCI, DMAP, CH₂Cl₂, r.t.; (c) i) CF₃COOH, CH₂Cl₂, r.t.; ii) **2b**, NaBH(OAc)₃, MeOH, r.t. (d) MeOH, NaBH(OAc)₃, r.t.; (e) *tert*-Butyl (4-bromobutyl)carbamate, K₂CO₃, TBAI, DMF, 60 °C; (f) CF₃COOH, CH₂Cl₂; (g) EDCI, DMAP, CH₂Cl₂, r.t.

phenyl group (**23g**). Comparable receptor binding was observed with the fragments 9*H*-carbazole-3-carboxamide (**23k**, D₃R $K_i = 144.7$ nmol/L) and quinoline-3-carboxamide (**23l**, D₃R $K_i = 85.7$ nmol/L), but quinoline-4-carboxamide led to the reduced binding activity. As can be seen with compounds **23a–m**, all (9-ethyl-9*H*-carbazol-3-yl)methanamine analogs with the linker composed of four carbon atoms exhibited slight inhibition of D₂R at 10 μmol/L (<15%), showing excellent D₃R selectivity profiles over D₂R.

To investigate the potential interactions of N-4 as well as improved physicochemical properties, an ethyl or propyl group was introduced to the N atom on the linker of bitopic ligands. However, compared to the original compounds **23a/23c/23j**,

alkylated derivatives were found to have less potential in D₃R binding affinity. For **23a**, the alkylation of the benzyl N atom unexpectedly increased the D₂R binding affinity (D₂R $K_i = 332.6$ nmol/L for **31a** and D₂R $K_i = 300.8$ nmol/L for **31c**) (Table 3). It is speculated that the alkylation of the benzyl N atom of **23a** changed the bitopic binding mode by turning the 1*H*-indole-2-carboxamide moiety into an OBS binding part.

Binding studies continued to evaluate the tetrahydro-carboline core structure to determine if the scaffold hopping was engaging D₃R affinity and selectivity. Regarding superior binding structures for SBP, aromatic carboxamide moieties were also explored in the tetrahydro-carboline scaffold to obtain the bitopic ligands and binding affinities were shown in Tables 4 and 5. Replaced by 1*H*-



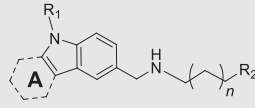
Scheme 3 Synthesis of carboline derivatives. Reagents and conditions: (a) AcOH, TsOH, reflux; (b) *tert*-butyl (4-bromobutyl)carbamate, K₂CO₃, TBAI, DMF; (c) i) CF₃COOH, CH₂Cl₂; ii) EDCI, DMAP, CH₂Cl₂; (d) (Boc)₂O, CH₂Cl₂; (e) MeI or CH₃CH₂I, NaH, THF, 0 °C; (f) CF₃COOH, CH₂Cl₂.

indole-2-carbamate, two tetrahydro- γ -carboline analogs (**36a/36k**) were found to have improved binding affinities ($K_i = 10.6$ and 15.5 nmol/L), and excellent D₃R selectivity profiles of which *N*-methyl or *N*-ethyl substituent at the tetrahydro-carboline showed no distinct difference. The same SAR was found for the tetrahydro- β -carboline analogs (**42a/b**). Ligand **36c** demonstrated a drastic decrease in D₃R binding affinity. Interestingly, due to the excellent D₃R binding properties observed with compounds **23i**, quinoline-3-carbamate (**36d**) was also explored, however it was found to dramatically reduced D₃R affinity. Almost all other aromatic carboxamide moieties replacements, as they are present in compound **36f-j**, led to the improved D₃R binding affinity, especially for **36f** and **36i** with an approximate K_i value of 4 nmol/L. Ligand **36g** ($K_i = 29.0$ nmol/L) was found to have a comparable binding affinity with **23j**. However, for the tetrahydro- β -carboline analogs (**42c/g/h**), D₃R affinities lost dramatically. Compared to the carbazole scaffold, tetrahydro-carboline

scaffold linked the 9*H*-carbazole-3-carbamate moiety (**36h**, $K_i = 19.6$ nmol/L and **42d**, $K_i = 36.7$ nmol/L) was more potential, affording an increase in D₃R binding. Compound **36j** ($K_i = 14.2$ nmol/L) with a tetrahydro- γ -carboline scaffold linked the 1*H*-benzo[*d*]imidazole moiety showed better binding affinity to D₃R than compounds with a tetrahydro- β -carboline scaffold (**42e**, $K_i = 203.0$ nmol/L and **42f**, $K_i = 300.0$ nmol/L). The same SAR was obtained from the tetrahydro- γ -carboline derivative **36i** ($K_i = 3.7$ nmol/L) and tetrahydro- γ -carboline derivatives (**42i**, $K_i = 112.0$ nmol/L and **42j**, $K_i = 149.0$ nmol/L).

2.5. Functional study by measuring *p*-ERK1/2 mediated D₃ receptor signaling

To access the fundamental activities of these novel D₃R selective ligands, *p*-ERK1/2 as the key molecular in signal transduction was tested. To ensure the reliability of the ERK1/2

Table 1 Binding affinities of compounds **3a–c**, **8**, **13** and **17a–f** at hD₂ and hD₃ receptors.


Compd.	A	R ₁	R ₂	% inhibition at 10 μmol/L		K _i (nmol/L) ^a	
				hD ₂	hD ₃	hD ₂	hD ₃
ZLG-25 (3b)		Et		17.6 ± 17.5	95.4 ± 3.0	>10,000 ^b	685.0 ± 4.5
3a		Me		13.4 ± 23.8	63.8 ± 8.0	NA	NA
3c		<i>i</i> Pr		1.7 ± 9.2	83.8 ± 10.2	>10,000 ^b	665.4 ± 13.5
8		H		33.2 ± 17.5	54.2 ± 7.7	NA	NA
13		H		15.7 ± 1.7	36.9 ± 2.1	NA	NA
17a		Et		-23.6 ± 18.6	75.6 ± 3.5	>10,000 ^b	994.1 ± 36.6
17b		Et		-24.6 ± 5.1	95.8 ± 6.9	>10,000 ^b	96.7 ± 13.4
17c		Et		30.5 ± 4.0	63.0 ± 5.2	NA	NA
17d		Et		71.8 ± 3.6	75.0 ± 14.5	>10,000 ^b	1104.5 ± 115.2
17e		Et		10.6 ± 7.4	-10.2 ± 13.3	NA	NA
17f		Et		12.8 ± 7.7	-7.9 ± 12	NA	NA

^aK_i values are taken from three experiments, expressed as means ± SEM.

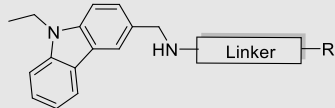
^bThe K_i values were not calculated because the inhibition percentages at 10 μmol/L were too low.

phosphorylation measurement assays to evaluate the functions to D_{2/3}R, several typical D_{2/3}R modulators were used as positive drugs. The results were shown in Supporting Information Fig. S4 that dopamine showed significantly increased level of pERK1/2 in CHO-hD₂R and CHO-hD₃R cells. Additionally, the full D_{2/3}R agonist, quinpirole at 20 μmol/L, induced a full ERK1/2 phosphorylation with the similar effects as dopamine. PD128907 was recognized as a D₃R-selective agonist with D₃R K_i of 1 nmol/L and D₂R K_i of 1183 nmol/L⁵⁰. As a positive control, PD128907 robustly stimulated a full ERK1/2 phosphorylation in CHO-hD₃R cells but not CHO-hD₂R cells indicating the D₃R selective agonism. As an antagonist or weak partial agonist, cariprazine and haloperidol did not exhibit significant effects to the ERK1/2 phosphorylation. GSK598809 (a highly D₃R selective antagonist, D₃R K_i = 2.9 nmol/L, D₂R K_i = 2110 nmol/L) was measured the ERK1/2 phosphorylation to D₂R and D₃R and found no significant effects. As shown in Fig. 3A, dopamine significantly increased the level of pERK1/2 in hD₃R-CHO cells, but compounds **23j**, **36a**, **36b** and **36f** were found no influence in the ERK1/2 phosphorylation to hD₃R by the compounds alone. Competitive antagonism assays in the present of 20 μmol/L dopamine were also performed, which showed compounds **23j**, **36a**, **36b** and **36f** could dose-dependently inhibit the ERK1/2 phosphorylation mediated by D₃R (Fig. 3C). From the results (Fig. 3B), we found that compounds

23j, **36a**, and **36b** showed weak partial agonism to D₂R at a high level. These compounds could inhibit the ERK1/2 phosphorylation induced by dopamine but not eliminate (Fig. 3D). Compound **36f** showed no functional affects to D₂R. The selected compounds with excellent D₃R binding affinity failed to stimulate ERK1/2 phosphorylation in CHO-hD₃R cells, which corroborated that the carbazole or tetrahydro-carboline D₃R selective ligands possessed no intrinsic agonistic activity and acted as D₃R antagonists. All the results indicated **23j**, **36a**, **36b** and **36f** as the D₃R-selective antagonists respectively with the IC₅₀ value of 17.7, 154.6, 594.4, and 673.9 nmol/L.

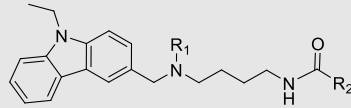
2.6. Binding modes analysis

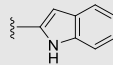
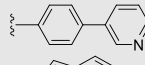
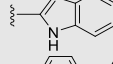
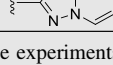
To explain the SARs of novel bitopic scaffolds, the representative compounds **23j**, **36b**, **36f** and **42a**, were docked into the OBS of the D₃R (PDB ID: 3pbl). The OBS was a hydrophobic pocket surrounded by aromatic residues (Phe188, Phe345, Phe346, His349, and Tyr365), where the hydrophobic carbazole moiety of compound **23j** deeply buried in (Fig. 4A). The aromatic carbazole structure of compound **23j** formed π-π interactions with Phe345, Phe346, and His349, and its hydrogen atom of NH⁺ at the benzyl position of the carbazole group formed an ionic hydrogen bond with Asp110. In the comparison with the carbazole moiety, the carboline region was similarly located at the OBS region

Table 2 Binding affinities of compounds **22a–c** and **23a–m** at hD₂ and hD₃ receptors.


Compd.	Linker	R	% inhibition at 10 μmol/L		<i>K_i</i> (nmol/L) ^a	
			hD ₂	hD ₃	hD ₂	hD ₃
22a			-4.8 ± 27.2	42.1 ± 2.2	NA	NA
22b			8.1 ± 3.9	21.3 ± 8.5	NA	NA
22c			22.4 ± 5.7	32.7 ± 11.4	NA	NA
23a			30.0 ± 14.1	87.0 ± 2.5	>10,000 ^b	62.6 ± 8.0
23b			-4.7 ± 14.2	86.7 ± 1.9	>10,000 ^b	577.6 ± 85.0
23c			-17.6 ± 2.0	98.4 ± 2.0	>10,000 ^b	45.7 ± 2.2
23d			2.7 ± 4.3	98.5 ± 2.3	>10,000 ^b	125.1 ± 17.6
23e			1.9 ± 10.7	99.2 ± 0.5	>10,000 ^b	99.3 ± 31.9
23f			5.5 ± 21.5	97.6 ± 0.3	>10,000 ^b	95.1 ± 8.9
23g			-15.9 ± 21.9	102.3 ± 1.2	>10,000 ^b	206.3 ± 2.9
23h			5.2 ± 7.6	105.0 ± 1.5	>10,000 ^b	24.2 ± 4.4
23i			6.5 ± 2.3	101.0 ± 0.8	>10,000 ^b	21.3 ± 4.3
23j			12.4 ± 5.8	107.3 ± 0.3	>10,000 ^b	13.9 ± 3.4
23k			10.6 ± 3.3	98.1 ± 0.8	>10,000 ^b	144.7 ± 11.9
23l			9.6 ± 0.1	100.0 ± 1.3	>10,000 ^b	85.7 ± 2.9
23m			-19.1 ± 5.8	63.1 ± 0.2	NA	NA
27			15.6 ± 3.0	88.9 ± 0.9	>10,000 ^b	52.1 ± 6.0

^a*K_i* values are taken from three experiments, expressed as means ± SEM.^bThe *K_i* values were not calculated because the inhibition percentages at 10 μmol/L were too low.

Table 3 Binding affinities of compounds **31a–e** at hD₂ and hD₃ receptors.


Compd.	R ₁	R ₂	% inhibition at 10 μmol/L		K _i (nmol/L) ^a	
			hD ₂	hD ₃	hD ₂	hD ₃
31a	Et		88.1 ± 1.5	96.2 ± 0.2	332.6 ± 3.6	134.3 ± 9.6
31b	Et		36.9 ± 2.1	78.5 ± 0.3	>10,000 ^b	421.8 ± 18.3
31c	<i>n</i> Pr		89.8 ± 2.9	98.6 ± 0.6	300.8 ± 11.9	448.2 ± 26.1
31d	<i>n</i> Pr		26.8 ± 0.9	81.3 ± 0.6	>10,000 ^b	994.4 ± 45.3
31e	<i>n</i> Pr		18.6 ± 2.5	74.8 ± 1.5	>10,000 ^b	478.2 ± 29.4

^aK_i values are taken from three experiments, expressed as means ± SEM.

^bThe K_i values were not calculated because the inhibition percentages at 10 μmol/L were too low.

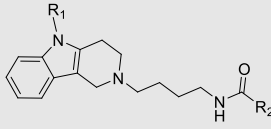
exhibiting fewer π -stacking interactions with Phe345, Phe346, and His349, which could be seen from **36b**, **36f**, and **42a** (Fig. 4B, Supporting Information Fig. S5A and S5B). The hydrogen atom of NH⁺ at the 2-position of the carboline group formed an ionic hydrogen bond with Asp110 to stabilize the OBS binding conformation. For the SBP region, the 4-(pyridin-3-yl) benzamide moiety was predicted docked to the SBP region on the edge of the whole pocket, indicating the bitopic binding mode. The hydrogen atom of the amide structure formed a hydrogen bond with Glu90, but pyridin-3-yl group was almost exposed to water due to the long linear structure of **23j**. The similar binding mode with **23j** was observed in **36f**, which [1,1'-biphenyl]-4-carboxamide moiety extended into solvents. 1*H*-benzo[*d*]imidazole-2-carboxamide of **36b** and 1*H*-indole-2-carboxamide of **42a** both offered the hydrogen bond formed between NH and Glu90, suggesting that interactions with Glu90 played key roles in the bitopic binding mode.

To verify the binding modes in a dynamic condition, 300 ns MD simulations for compounds **23j**, **36b**, and **36f** and **42a** were performed with Desmond software. Compound **23j** exhibited unstable binding conformation with the fluctuant ligand RMSD (Supporting Information Fig. S6A) and therefore the entire MD of 300 ns was analyzed. The complexes of compound **36b** were stable after 30 ns from the beginning of simulations (Fig. S6B), and then the trajectories from 50 to 150 ns were extracted and analyzed. The MD analysis of **23j** were shown in Fig. 4C and E, indicating consistent results with docking. The stable interactions between Asp110 and NH₂⁺ at the benzyl position of the carbazole group existed during 98% of the simulation time as the H-bond or ionic bond. The aromatic carbazole was predicted to form abundant hydrophobic interactions with Phe345, Phe346, and His349 in the 65%, 74%, and 85% stimulation time, respectively, indicating that the hydrophobic carbazole group could stabilize the OBS of hD₃R. Nevertheless, the 4-(pyridin-3-yl)benzamide moiety of **23j** seemed to broadly interact with the amino acids at the gorge entrance, such as Val86, Glu90, Tyr365, Ser366, Thr369, and Tyr373. The group embedded in the SBP span freely in the solvent in the absence of possible stabilizing interactions, which

might explain the fluctuant RMSD of the whole system. The MD analysis of **36b** showed (Fig. 4D and F), that the carboline region of **36b** was well embedded in the OBS forming stable interactions with Asp110 during 75% of the stimulation time as the H-bond, ionic bond, or water-bridge. Compared with **23j**, the ionic bond formed by **36b** with Asp110 seemed more prominent in all its interactions. However, fewer hydrophobic interactions by π - π stacking were predicted for the carboline group than for the carbazole group. The same situation appeared to the SBP binding moiety of **36b** viz., fewer interactions were observed during the extracted stimulation time. The SBP binding with 1*H*-benzo[*d*]imidazole-2-carboxamide significantly contributed to the stable conformation, especially the specific interactions with Glu90, which played a key role in about 60% time, such as H-bonds and water bridges. Unfortunately, the conformation of hD₃R with **36b** or **42a** was constantly perturbed during the 300 ns MD, and it was difficult to analyze a more stable conformation (Fig. S6C and D).

2.7. Binding selectivity profiles

The interactions between representative compounds and other receptors related to psychotic disorders were evaluated, and a selectivity profile was created using additional receptors (including hDR₁₋₅, h5-HT_{1A}, h5-HT_{1B}, h5-HT_{2A}, h5-HT_{2C}, h5-HT₆, hH1, h α 1 receptors, Dopamine Transporter (hDAT), Norepinephrine Transporter (hNET), Serotonin Transporter (hSERT)) to investigate its potential off-target activity. As shown in Table 6, both selected compounds showed the highest affinity to the D₃R receptor (**23j** K_i = 16.8 nmol/L; **36b** K_i = 19.6 nmol/L) in the dopamine receptor families. Compound **23j** displayed a relatively higher affinity to the 5-HT_{1B} receptor (K_i = 172.2 nmol/L). The other selected compound **36b** exhibited comparable selectivity to D₃R over 5-HT_{1B} receptor (K_i = 138.0 nmol/L). Furthermore, **23j** and **36b** showed the comparatively potential binding activity to 5-HT_{1A} receptor, and 5-HT_{2A} receptor. To hD₂R, h5-HT_{2C} receptor, h5-HT₆ receptor, hNET, hDAT and hSERT, both **23j** and **36b** showed weak binding affinity (K_i > 2000 nmol/L). Overall, compounds **23j**

Table 4 Binding affinities of compounds **36a–k** at hD₂ and hD₃ Receptors.


Compd.	R ₁	R ₂	% inhibition at 10 μmol/L		K _i (nmol/L) ^a	
			hD ₂	hD ₃	hD ₂	hD ₃
36a	Me		20.9 ± 3.8	97.6 ± 2.0	>10,000 ^b	10.6 ± 4.5
36b	Me		19.6 ± 5.7	97.9 ± 3.6	>10,000 ^b	16.8 ± 1.8
36c	Me		21.1 ± 9.0	66.3 ± 9.1	NA	NA
36d	Me		15.6 ± 12.9	42.5 ± 6.8	NA	NA
36e	Me		-2.0 ± 17.4	68.1 ± 1.9	NA	NA
36f	Me		-20.7 ± 4.9	103.5 ± 1.4	>10,000 ^b	4.1 ± 0.3
36g	Me		29.2 ± 5.8	83.8 ± 12.7	>10,000 ^b	29.0 ± 3.3
36h	Me		74.4 ± 3.3	95.5 ± 0.7	NA	19.6 ± 7.3
36i	Me		38.9 ± 3.8	87.5 ± 6.1	>10,000 ^b	3.7 ± 0.6
36j	Me		27.7 ± 1.4	74.4 ± 8.2	>10,000 ^b	14.2 ± 0.7
36k	Et		13.2 ± 7.3	105.5 ± 2.2	>10,000 ^b	15.5 ± 1.8

^aK_i values are taken from three experiments, expressed as means ± SEM.

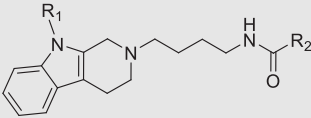
^bThe K_i values were not calculated because the inhibition percentages at 10 μmol/L were too low.

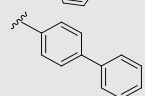
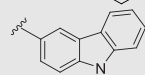
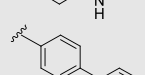
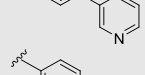
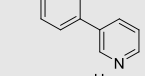
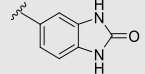
and **36b** showed excellent *in vitro* selective profiles with a preferred affinity for the D₃R.

2.8. Pharmacokinetic profiles and brain penetration properties study

Pharmacokinetics profiles of the selected compounds were extensively studied in ICR mice by i.v. administration at 3 mg/kg and *p.o.* administration at 10 mg/kg. As shown in Supporting Information Fig. S7, the plasma concentrations of each compound were monitored for 24 h. The related profiles were calculated and shown in Table 7. Both compounds showed a rapid distribution (T_{\max} = 0.17 and 0.25 h for **23j** and **36b**) at a dose of 10 mg/kg (*p.o.*). Nevertheless, compound **36b** showed a much more effective blood plasma concentration (C_{\max} = 505.2 ng/mL)

comparable to that of compound **23j** (C_{\max} = 78.8 ng/mL) for the *p.o.* administration. Similarly, the C_{\max} of the i.v. administration for compound **36b** was found to be more than one-fold higher than **23j**. Compounds **23j** and **36b** had the comparable half-life ($t_{1/2}$ = 1.1 h) for 10 mg/kg *p.o.* administration. Finally, the oral bioavailability of **23j** was rather low and did not reach a sustained pharmacologically relevant plasma concentration during an oral dosing period. Despite the high on-target potency and good selectivity for the carbazole scaffold, the results of **23j** indicated its poor PK profile (high i.v. clearance and no oral bioavailability). After hopping to the tetrahydro-carboline structure, the oral bioavailability seemed to be greatly improved, as can be seen from compound **36b** (F = 39.7%), by which the lower i.v. clearance was accompanied, perhaps due by its lower first-pass metabolism. Further tests for their brain penetration

Table 5 Binding affinities of compounds **42a–j** at hD₂ and hD₃ receptors.


Compd.	R ₁	R ₂	% inhibition at 10 μmol/L		K _i (nmol/L) ^a	
			hD ₂	hD ₃	hD ₂	hD ₃
42a	Me		9.1 ± 16.4	106.3 ± 1.3	>10,000 ^b	6.8 ± 0.8
42b	Et		17.5 ± 1.5	105.5 ± 3.6	>10,000 ^b	12.9 ± 2.1
42c	Et		-9.1 ± 20.7	63.9 ± 7.0	NA	NA
42d	Et		19.2 ± 8.3	97.1 ± 2.9	>10,000 ^b	36.7 ± 1.5
42e	Me		49.7 ± 1.2	81.5 ± 0.6	NA	203.0
42f	Et		54.1 ± 0.1	80.6 ± 1.1	NA	300.0
42g	Me		37.8 ± 1.0	69.6 ± 0.8	NA	NA
42h	Et		28.9 ± 0.8	31.3 ± 0.6	NA	NA
42i	Me		37.6 ± 0.2	85.2 ± 0.5	NA	112.0
42j	Et		48.8 ± 0.7	85.9 ± 0.07	NA	149.0

^aK_i values are taken from three experiments, expressed as means ± SEM.

^bThe K_i values were not calculated because the inhibition percentages at 10 μmol/L were too low.

properties were performed at 0.5 and 2.0 h, and the brain/plasma ratios were calculated. The results showed that the brain/plasma ratio of **23j** was lower than one at 0.5 h after one single administration (3 mg/kg i.v.) and reached 1.5 at 2.0 h due to lower clearance in the brain. When analyzed after a single oral administration, the concentration of compound **23j** in the brain was too low to test. The BBB permeability of compound **36b** was found to be prominent after a single i.v. administration achieving a brain/plasma ratio high to 4.5 at 0.5 h, and this ratio was maintained at a high level above five until 2.0 h. Notably, the brain concentration of compound **36b** rapidly reached 1553 ng/mL, which was higher than the i.v. C_{max}. Considering the brain/plasma ratio after a single oral administration was calculated from 0.74 to 0.97, compound **36b** seemed to provide a moderate brain exposure (from 310 to 180 ng/mL). As can be seen from the pharmacokinetic profiles of **23j**, the carbazole derivatives may have a poor oral bioavailability. Then, in order to obtain candidate potential compounds in the next catalepsy tests and hyperactivity tests, i.p. administration was processed to evaluate the major therapeutic effects and side effects.

2.9. hERG channel blockade and cytotoxicity tests

Unwanted inhibition of the hERG channel can induce severe cardiac arrhythmias, such as long QT syndrome characterized by prolonged QT intervals and Torsades de pointes⁵¹. The inhibition of the hERG channel of the selected compounds was further tested by patch-clamp assays to predict cardiovascular toxicity (Supporting Information Fig. S8)⁵². As the results are shown in Table 8, RPD and compounds **23j**, **36a**, **36b**, **36f** were tested for their blockage to hERG showing the IC₅₀ as 96, 2620, 1410, 1750, and 46,950 nmol/L, respectively. Compound **36f** (hERG IC₅₀ > 40 μmol/L) exhibited good safety profile in terms of cardiotoxicity. Compound **23j** had a lower hERG inhibition than the others. Furthermore, **36a** showed potential selectivity to D₃R compared with hERG. Compound **36b** was found to have higher hERG inhibition but still had a comparative advantage *versus* RPD (hERG IC₅₀ = 96 nmol/L as tested at the same conditions). Next, further cytotoxicity tests to evaluate the safety of candidates were performed in HEK293T, BV2 and PC12 cells. The results were shown in Supporting Information Fig. S9 indicating that **36b** and

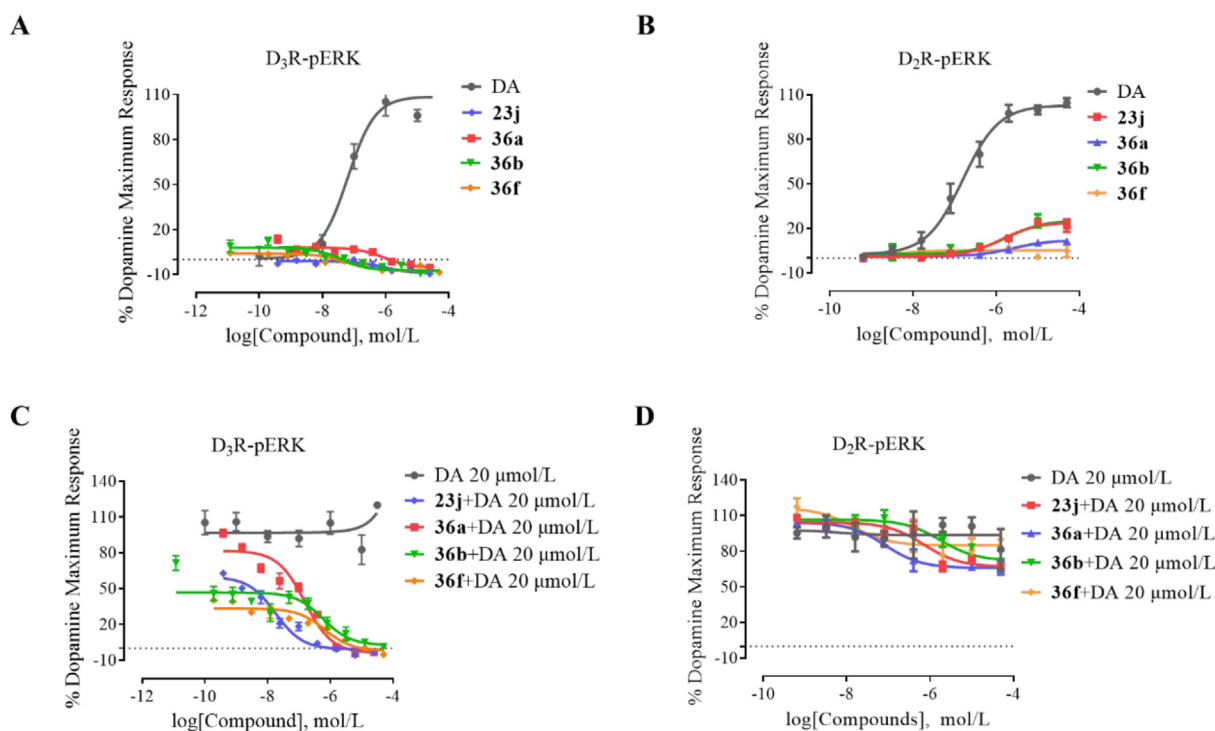


Figure 3 Functional characterization of lead compounds at D_3 dopamine receptors by ERK1/2 phosphorylation measurement. (A) Agonist dose–response curves for ERK1/2 phosphorylation mediated by hD_3R and (B) ERK1/2 phosphorylation mediated by hD_2R ; (C) Competitive antagonist dose–response curves for ERK1/2 phosphorylation mediated by hD_3R and (D) ERK1/2 phosphorylation mediated by hD_2R in the present of 20 $\mu\text{mol/L}$ dopamine.

36f exhibited less effects on the viability of HEK293T and BV2 than that of RPD. In PC12 cells, **36b** shown the best safety profiles. But compounds **23j** and **36a** unexpectedly exhibited significant cytotoxicity at high concentrations.

2.10. Acute toxicity assays and catalepsy tests in mice

One of the major obstacles to using antipsychotics is their propensity to produce extrapyramidal motor side effects. The catalepsy tests were used to detect the extrapyramidal side effects in mice during the antipsychotic drug discovery^{53,54}. But before catalepsy tests, preliminary acute toxicity assays in mice were performed to observe the maximum tolerated dose for the tested compounds as before⁵⁵. All mice were intraperitoneally injected with tested compounds and persistently observed for 24 h. The results were presented in Supporting Information Table S6, and compounds **36b** and **36f** were found well tolerant even at the highest concentration (600 mg/kg, i.p.). Compound **23j** showed a dose-dependent lethal toxicity from 240 to 600 mg/kg. For the dose of 240 mg/kg or above, the serious death often occurs after 12 h. As the example of **36f**, it took doses of 480 mg/kg or above to cause death in individual mice. Known the maximum tolerated dose for the tested compounds, catalepsy was then tested on each compound with increasing concentration gradients by i.p. administration⁵⁶. The number of the mice with cataleptic reaction in each group was recorded. The ED_{50} , minimum effective doses (MED), and peak effects (percent of cataleptic animals) were accordingly calculated. As shown in Table 8, RPD was used as the positive control drug and induced a significant cataleptic effect from 2.4 mg/kg. It was found that almost all mice exhibited catalepsy at the high concentrations of RPD, while the ED_{50} was

approximately 1.51 mg/kg, which was related with its solid antagonistic effect on the D_2R . In contrast, compounds **23j**, **36a**, **36b** and **36f** did not elicit catalepsy under all tested doses (i.p.). The highest safe dose of **23j** was found between 240 and 480 mg/kg (i.p.) since 240 mg/kg (i.p.) induced no catalepsy but 480 mg/kg (i.p.) was lethal for mice. 480 mg/kg (i.p.) for **36a/b/f** was found to be safe, and no higher dosage was investigated, considering its effective dose of 10–30 mg/kg. These results showed that this series of D_3R -selective ligands had a high threshold for catalepsy, which was associated with its low affinity to D_2R .

2.11. MK-801-induced hyperactivity tests and apomorphine-induced climbing tests of selected compounds

Schizophrenia is a heterogeneous disorder with positive symptoms (delusions, hallucinations, thought disorders), negative symptoms (anhedonia, avolition, social withdrawal, poverty of thought), and cognitive dysfunction^{57,58}. But understanding of the biological origins of schizophrenia was still limited. Increased locomotor activity in response to psychotomimetic compounds such as apomorphine or noncompetitive *N*-methyl-D-aspartate (NMDA) glutamate receptor antagonists is commonly used as an indication of positive symptoms in schizophrenia⁵⁹. It is well-known that, as an uncompetitive NMDA receptor antagonist, MK-801 could induce schizophrenic symptoms in healthy subjects and exacerbate existing psychoses in patients with schizophrenia⁶⁰. So as the past research, MK-801-induced hyperactivity tests were used for relatively high-throughput evaluation of the candidate compounds in our study^{47–49}. Selected compounds were tested in this model of ICR mice, before which the influences on the locomotion of selected compounds were firstly determined to avoid potential

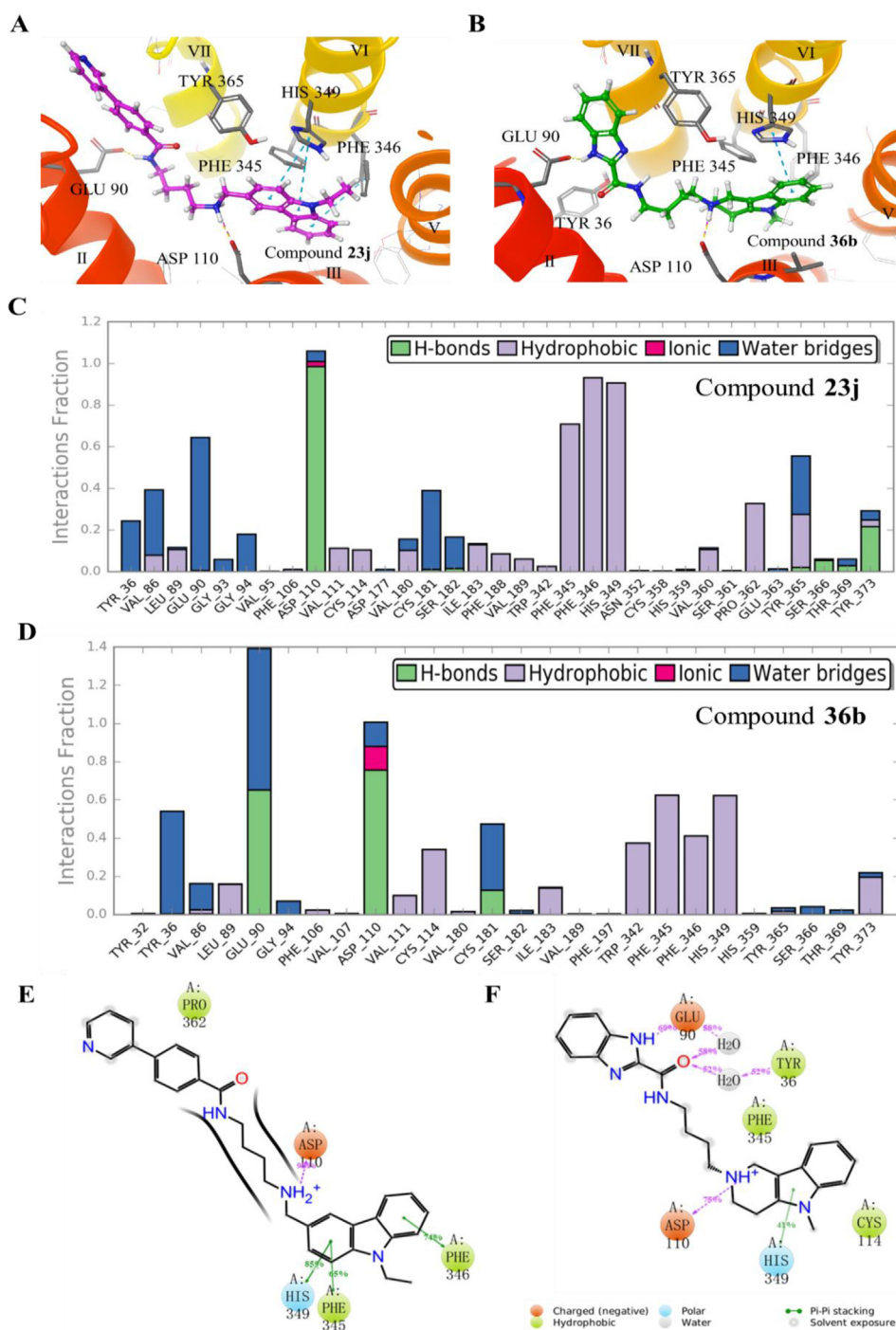


Figure 4 Binding modes analysis of **23j** and **36b**. (A) Predicted binding modes of compound **23j** with D₃R and (B) predicted binding modes of **36b** with D₃R. Images depicting the proposed binding modes were generated using Maestro software. Protein is shown as a cartoon, and small molecules are shown as sticks. Hydrogen bonds, π - π stacking interactions, and electrostatic interaction are depicted by yellow, purple, and blue dashed lines, respectively. Residues of D₃R interacting with ligands are depicted by green sticks. (C) Protein–ligand contacts histograms of D₃R with **23j** and (D) protein–ligand contacts histograms of D₃R with **36b**. (E) Corresponding 2D interaction diagrams of **23j** and (F) corresponding 2D interaction diagrams of **36b** predicted through MD simulations; percentage suggests that for X% of the simulation time, the specific interaction is maintained.

psychotic side effects. Spontaneous locomotor results recorded for 15 min indicated that all tested compounds (**23j**, **36a**, **36b** and **36f**) showed no influences at 30 mg/kg i.p., and RPD (1 mg/kg) was tested as the positive drug showing a moderate inhibition (Fig. 5B). In the following tests, the process was shown in Fig. 5A

indicating that compounds and vehicle were administrated i.p. and followed by the s.c. administration of MK-801 (0.3 mg/kg) 10 min later. Then, the moving distance of mice in the next 60 min was recorded. As the results shown in Fig. 5C–H, MK-801 group was significantly longer compared with the control group. As the

Table 6 Binding affinities of compounds **23j** and **36b** for inhibiting radioligand binding to antischizophrenic drugs targets.

Targets	23j K_i (nmol/L) ^a	36b K_i (nmol/L) ^a	Targets	23j K_i (nmol/L) ^a	36b K_i (nmol/L) ^a
hD ₁	> 10,000.0	> 10,000.0	h5-HT _{2C}	2230.0	5611.0
hD ₂	> 10,000.0	> 10,000.0	h5-HT ₆	8718.0	10,289.1
hD ₃	16.8	19.6	hH1	5197.7	2314.5
hD ₄	> 10,000.0	8813.0	h α 1	8353.1	2218.0
hD ₅	> 10,000.0	> 10,000.0	hDAT	6097	1062.9
h5-HT _{1A}	578.7	274.5	hNET	> 10,000.0	> 10,000.0
h5-HT _{1B}	172.2	138.0	hSERT	5411.0	> 10,000.0
h5-HT _{2A}	214.4	398.2			

^a K_i (nmol/L) values for the indicated compounds were determined as described in the Experimental Section.

Table 7 Pharmacokinetic and brain penetration properties of compound **23j** and **36b** in ICR mice ($n = 3/\text{group}$).

Parameters	Single-dose administration			
	3 mg/kg (i.v./ 23j)	10 mg/kg (p.o./ 23j)	3 mg/kg (i.v./ 36b)	10 mg/kg (p.o./ 36b)
C_{\max} (ng/mL)	566.80	78.80	1226.50	505.20
T_{\max} (h)	0.08	0.17	0.08	0.25
$t_{1/2}$ (h)	0.53	1.17	0.87	1.14
AUC _{0-t} (h·ng/mL)	325.50	94.40	677.30	896.30
CL (mL/h/kg)	9208.50	—	4421.50	—
MRT _(0-t) (h)	0.48	0.87	0.51	1.70
V_{dss} (mL/kg)	4439.60	—	2329.90	—
F	—	8.70	—	39.70
Brain concentration at 0.5 h (ng/mL)	98.04	—	1552.86	310.17
Plasma concentration at 0.5 h (ng/mL)	179.70	53.40	345.20	420.90
Brain/plasma ratio at 0.5 h	0.55	—	4.50	0.74
Brain concentration at 2.0 h (ng/mL)	11.48	—	138.55	181.65
Plasma concentration at 2.0 h (ng/mL)	7.17	2.89	24.87	188.03
Brain/plasma ratio at 2.0 h	1.60	—	5.57	0.97

positive drugs, RPD and CRP dose-dependently inhibited the MK-801-induced hyperactivity in our tests, and RPD showed more effective than CRP. Dose-dependent tests for **23j/36a/36b/36f** were performed at the doses of 3, 10, and 30 mg/kg. For all the tested carbazole derivatives, the dose of 30 mg/kg was found to be effective in the inhibition of MK-801-induced hyperactivity but not the spontaneous locomotion. Comparably, RPD by 1 mg/kg resulted in a significant inhibition of both spontaneous locomotion and MK-801-induced hyperactivity. Administration of 10 mg/kg was found effective ($P < 0.001$) for all derivatives, but the dose of 3 mg/kg did not show the inhibition activity at compounds **23j** and **36a**. Nevertheless, **36b** and **36f** administered i.p. at 3 mg/kg reduced the distance of mice movement compared with the MK-801 group ($P < 0.001$), suggesting the most potent inhibition of voluntary activity.

The antagonism of hyperlocomotion induced by dopamine receptor direct agonists (e.g., apomorphine) is used to evaluate the antipsychotic efficacy⁶¹. Apomorphine-induced climbing tests could determine the attenuation of climbing behavior induced by apomorphine in mice for identifying potential antipsychotic activity. In this test, RPD and CRP exhibited dose-dependent inhibition to the apomorphine-induced climbing behavior (Fig. 5I and J). The concentration gradient as three times as RPD was set for the treatment with compounds **23j** and **36b**, showing that both compounds could dose-dependently inhibit the apomorphine-

induced hyperactivity (Fig. 5K and L). The results indicated that potent D₃R antagonism could significantly decrease the effects of apomorphine linked to behavioral agitation, one positive psychotic symptom.

2.12. Antidepressant effects of compound **36b**

Regarding the exact nature relationship between depression and negative symptoms in a 'non-affective' psychotic illness such as schizophrenia⁶², models of behavioral despair such as forced swimming test (FST) and tail suspension test (TST), were used to evaluate the negative symptom-like behavior in lots of reported works^{63–65}. But due to limited antipsychotic drugs approved for depression, such as CRP, lurasidone, and quetiapine, there is a special significance to evaluating the antidepressant effects of antipsychotic compounds. In our study, considering more convincing safety, **36b** was further selected for more animal models of antipsychotic-drug-like activity and administered by p.o. because of its satisfactory oral bioavailability. We continued investigating the antidepressant effects of **36b** using the FST and TST. The FST is widely used to study depressive-like behaviors in rodents; in this test, the rodent's immobility time and latency by first observed immobility reflect a measure of behavioral despair. TST is another measure of behavioral despair sensitive to a broad range of antidepressant drugs that makes it a suitable

Table 8 hERG channel inhibition and catalepsy induced by RPD and selected compounds^a.

Compd.	hERG inhibition IC ₅₀ (nmol/L) ^b	Catalepsy		
		ED ₅₀ i.p. (mg/kg) ^b	MED i.p. (mg/kg) ^b	Peak effect (%) ^b
RPD	96.0	1.5	2.4	100.0
23j	2460.0	NT ^c	≥240.0	0.0
36a	1315.0	NT	≥480.0	0.0
36b	1750.0	NT	≥480.0	0.0
36f	46,950.0	NT	≥480.0	0.0

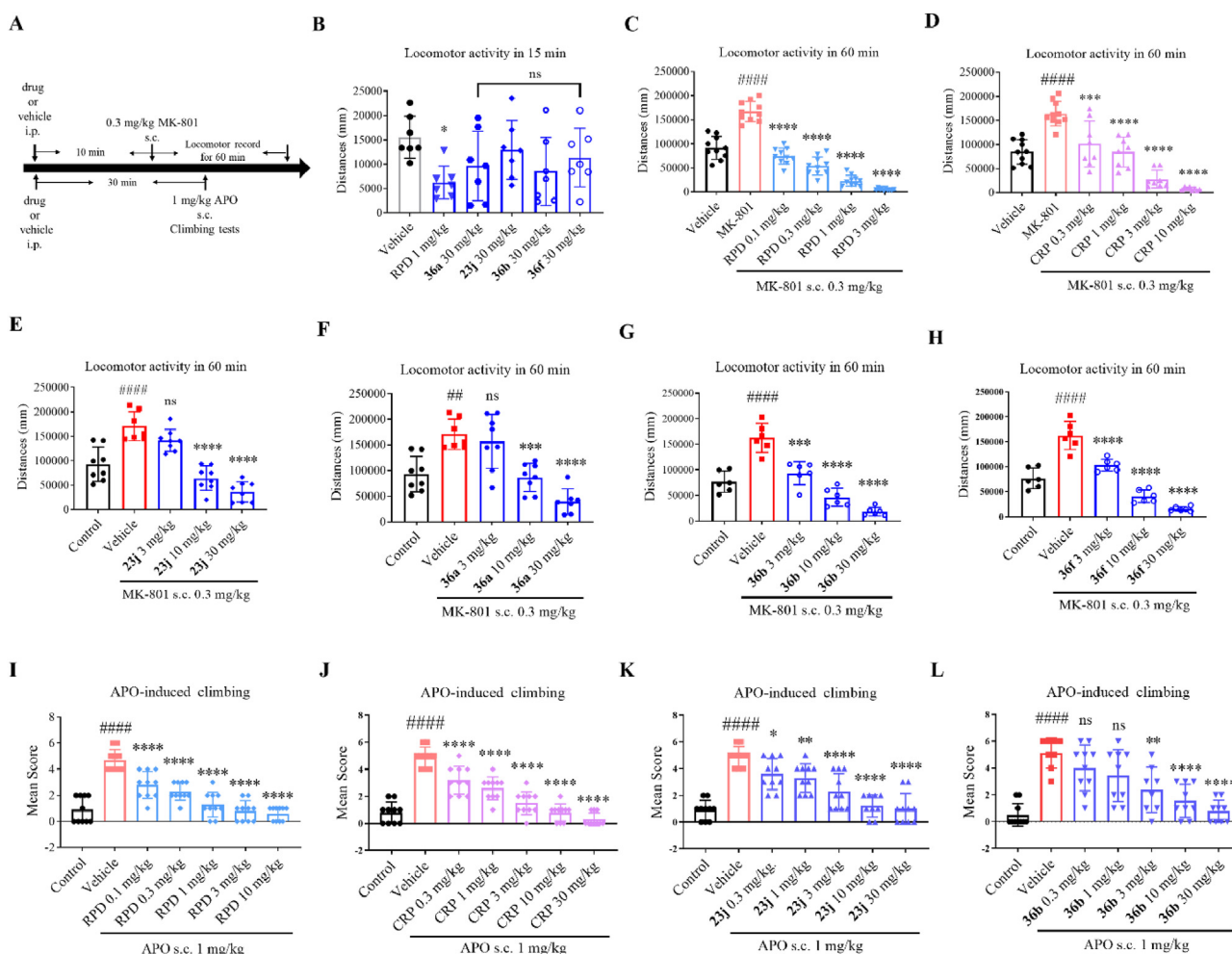
^aED₅₀, Minimum effective doses (MED), and maximal effects (percent of cataleptic animals) are shown.

^bAll values were tested for three times.

^cNot tested.

screening test. In our tests, duloxetine (DLX), considered one of the most effective antidepressant drugs in clinical practice, was used as the positive control. Administration of DLX caused a robust decrease in the immobility time in FST and TST, demonstrating its extraordinary antidepressant effect. Once

intraperitoneal treatment with compound **36b** dose-dependently decreased the immobility time in the TST compared with the control group ($P < 0.05$), but 3 mg/kg group did not show significant differences (Fig. 6A). For the latency by first observed TST immobility, only 30 mg/kg group was found to be prolonged



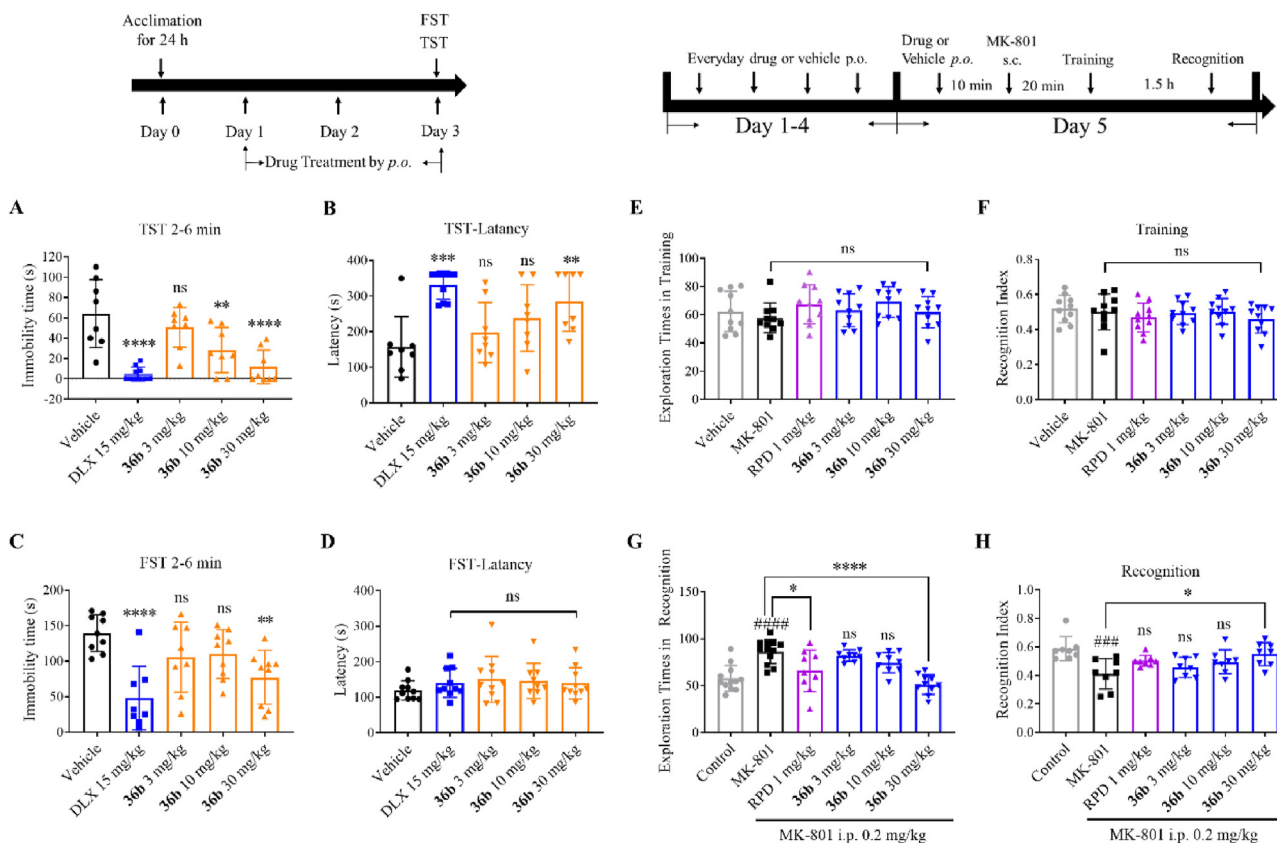


Figure 6 Evaluation of compound **36b** in animal models of behavioral despair and cognitive deficit. (A–B) Effects of compound **36b** (3, 10, 30 mg/kg) in the ICR mice TST ($n = 8–10$ /group). (C–D) Effects of compound **36b** (3, 10, 30 mg/kg) in the ICR mice FST ($n = 8–10$ /group). Effects of compound **36b** (3, 10, 30 mg/kg) on MK-801-induced object recognition disruption in mice ($n = 8–10$ /group). (E) Exploration times in the training and (F) the recognition index in exploring the same objects were scored ($n = 8–10$ /group). (G) Exploration times in the acquisition trial and (H) the novelty discrimination index (NDI) in exploring a familiar and novel object during acquisition trials (after 24 h training) were scored ($n = 8–10$ /group). Results are expressed as the means \pm SEM of distance traveled. Statistical evaluation was performed by one-way ANOVA followed by Dunnett's test for multiple comparisons. ### $P < 0.005$ and #### $P < 0.0001$ versus control group; *** $P < 0.001$ and **** $P < 0.0001$ versus vehicle group.

(Fig. 6B). So as immobility time of FST, 30 mg/kg group showed activities, but lower dose groups did not (Fig. 6C). DLX and compound **36b** failed to prolong the FST latency (Fig. 6D). The results indicated that compound **36b** exhibited potential antidepressant-like activity.

2.13. Effects of compound **36b** on MK-801-induced novel object recognition (NOR) disruption in mice

Cognitive deficit is considered a core feature of schizophrenia, and it lacks responsiveness to many current antipsychotic drugs. NOR is a form of visual-recognition memory dependent on animals' innate preference to investigate novel objects, which is decreased in schizophrenia patients because of their visual-recognition memory impairments⁶⁶. NOR models have been widely used to assess procognitive effects as quick, and straightforward preclinical models. The current study found that MK-801 could induce cognitive impairment in schizophrenia, consistent with previous reports disrupted NOR⁶⁷. During this study, compound **36b** and RPD were administered intraperitoneally for four days before the acquisition trial. On the fifth day,

1 h after administration, the training trial was performed by recording the exploration time for the two identical objects A. Then, 1.5 h later, one of the objects A was replaced by a novel object B for the recognition trial. During the training trial, no difference was found among the vehicle, MK-801, RPD, or **36b** groups in the total object exploration time (Fig. 6E). Moreover, the recognition index, which was calculated as the percentage of novel object interaction time relative to total interaction time during the retention trial, was indiscriminate for all groups (Fig. 6F). In the testing session (Fig. 6G), total interaction time to objects A and B was increased significantly for the MK-801 group compared with control due to MK-801-induced hyperactivity. As shown in Fig. 6H, the control group of mice spent more time exploring the novel object than the familiar object. In contrast, throughout the experiment, MK-801 (0.2 mg/kg, i.p.)-treated mice spent less time exploring the novel object, indicating that MK-801 treatment resulted in a cognitive deficit. The deficit in NOR index induced by MK-801 was alleviated by **36b** (30 mg/kg, i.p.) but not RPD (1 mg/kg). These results suggested that compound **36b** improved cognitive ability during the NOR tasks in mice.

2.14. Weight gain and serum prolactin

The potential adverse effect profile was also assessed in terms of its ability to induce weight gain and high prolactin levels. Successive *p.o.* administrations of the compounds **23j** and **36b** at 30 mg/kg were performed for 30 days (one time/day). The positive group was administered with 1 mg/kg RPD and control group was treated with vehicle in the same process. The Body weight for each mouse was recorded every day. No influence on body weight was observed for either compound compared with the control (Supporting Information Fig. S10A). Nevertheless, weight gain trends and the daily behavior of **23j** and **36b** administration groups were unaffected. The weight gain of RPD group grew obviously faster 15 days later from the beginning. Moreover, after 30 days of dosing, RPD raised the serum prolactin level but compounds **23j** and **36b** resulted in nonsignificant serum prolactin change (Fig. S10B). These results suggested that both compounds displayed a remarkable safety profile.

3. Conclusions

The D_{2/3}R binding affinities and functional selectivity have been studied for decades to explore the benefits for treating the schizophrenia. Highly D₃R selective antagonists exhibited some promising profiles in mood regulation, cognitive protection, and low side effects. We aimed to develop novel D₃R selective ligands with improved *in vivo* activity and drug properties for further development as clinical antipsychotics. Starting with virtual screens, a series of carbazole and tetrahydro-carboline derivatives were obtained through bitopic design and scaffold hopping strategy. A large proportion of compounds with the carbazole scaffold exhibited excellent binding affinities for the D₃R with good selectivity against D₂R. The tetrahydro- γ -carboline derivatives were found improved in D₃R binding affinities, but the tetrahydro- β -carboline showed less potential. In the functional studies, D₃R antagonism and weak D₂R partial agonism were identified for the novel ligands. Among the derivatives, compounds **23j** and **36b** were selected as our lead compounds, showing a moderate selectivity to D₃R over 5-HT_{1A}, 5-HT_{1B}, and 5-HT_{2A} receptors and a weak affinity to the D₂, 5-HT_{2C}, and 5-HT₆ receptors. Binding mode analysis verified the scaffold hopping strategy's feasibility and understanding of the bitopic binding to D₃R. According to the data in MK-801-induced hyperactivity and catalepsy tests, these new D₃R selective antagonists were all effective in inhibiting the hyperactivity without cataleptic reactions. Further, compounds **23j** and **36b** dose-dependently reduced apomorphine-induced hyperactivity without cataleptic reaction. Compound **36b** also possessed unusual antidepressant-like activity in the FST and the TST. Moreover, compound **36b** alleviated the MK-801-induced disruption of novel object recognition in mice. Furthermore, the PK/PD studies of the compound **36b** in mice displayed superior profiles, including moderate drug exposure and excellent brain penetration properties. In addition, compound **36b** exhibited promising safety profiles in long-term drug administration without serum prolactin levels and weight gain change. Taken together, the results supported **36b** as a suitable lead compound, and additional investigation for developing **36b** into a promising pharmacotherapeutic for the treatment of psychoses is needed.

4. Experimental

4.1. Virtual screening and induced-docking

4.1.1. Ligand-based virtual screening

Pipeline Pilot 8.5 of Accelrys was used to perform all of the similarity searches⁴⁶. The fingerprint ECFP₆ was generated for each structure of (R)-PG648, RGH-188, and GSK598809, then similarities were calculated using Tanimoto coefficient. Then, more than 9000 analogs were identified for further screening.

4.1.2. Structure-based virtual screening

Dopamine D₃ receptor crystal structure (PDB ID: 3pbl) was selected for the study *in silico*. Afterward, the D₃R structures was prepared by the Protein Preparation Wizard module in Schrodinger 10.2 software. The protein was assigned bond orders, added hydrogens, protonated, removed all crystallographic water molecules, and restrained minimization. Then, the eticlopride was docked into prepared model to check the reasonability for further docking screen. In next step, approximately more than 9000 compounds obtained from the similarity search were prepared to generate conformations by the LigPrep module of the Schrodinger suite (Schrodinger, NY, USA). Then, energy-minimized conformations were docked into the eticlopride binding site of the crystal structure. Then, three predicted binding poses were generated for each compound. According to the score obtained by the extra precision (XP) scoring function of the Glide module, 831 compounds (XP GScore < -9) were retained. The remaining 490 compounds were selected after structurally clustered into 26 clusters based on the Tanimoto coefficients computed using the ECFP₆ fingerprint. Lastly, 65 candidate compounds were purchased for further evaluation by radioligand competition binding assays.

4.1.3. Induced-docking

The prepared crystal structure (PDB ID: 3pbl) was used in the Induced Docking module with XP. For ligand preparation, conformations of ZLG-25, **23j** and **36b** were generated and energy-minimized by the LigPrep module. Images depicting the proposed binding modes were generated using Maestro 11.5.

4.2. Molecular dynamics simulations

Following molecular docking, 200 ns MD simulations for ZLG-25, 300 ns MD simulations for **23j** and **36b** were performed ligand-protein complex using the Desmond software⁴⁶. According to the membrane position loading from the Orientations of Proteins in Membranes (OPM) database, D₃R crystal structure (PDB ID: 3pbl) was accurately set up to the phospholipid bilayer⁶⁸. Na⁺ and Cl⁻ ions were added at the physiological concentration of 0.15 mol/L to ensure the overall neutrality of the systems. Simulations were conducted with an OPLS3 force field and a TIP3P explicit solvent model. We chose a 4.8 ps recording interval, and the NPT ensemble was employed with temperature fixed at 300 K and pressure at 1.01 bar. The integration time step was set at 2 fs. The model systems were relaxed using a six-step default protocol implemented in Desmond and utilized to prepare systems for production quality simulation. Default settings were used for all other parameters. The simulation interaction diagram analysis tool was used to monitor energetics, RMSD fluctuations,

hydrogen-bond distances, angles, and van der Waals interactions over the simulation trajectories.

4.3. Chemical synthesis

All commercially available reagents and solvents were used without further purification. Reactions were monitored by thin-layer chromatography (TLC) on precoated glass silica gel plates (GF254, 0.25 mm, Yantai Xinde Chemical Co., Ltd.) using a $\text{CH}_2\text{Cl}_2/\text{MeOH}/50\%$ aq NH_4OH system or an $\text{EtOAc}/\text{petroleum ether}$ system. Column chromatographic purification was carried out using silica gel. Melting points were determined using an X-4 micro melting point apparatus. ^1H NMR and ^{13}C NMR spectra were recorded on a Bruker Avance III 400 spectrometer using chloroform-*d* or DMSO-*d*₆ as the solvent. *J* values were reported in hertz (Hz). Chemical shifts were given in δ values (ppm), using tetramethylsilane (TMS) as the internal standard. Signal multiplicities are characterized as the following abbreviation: s (singlet), d (doublet), t (triplet), q (quartet), m (multiplet), and br (broad signal). All final test compounds' purity is determined by highperformance liquid chromatography (HPLC), and all final test compounds display purity higher than 95%. HPLC methods used the following: Waters LC-20 AD spectrometer; Waters Xbridge BEH Amide column (4.6 mm \times 250 mm, 5 $\mu\text{mol/L}$ i.d.); mobile phase, H_2O aq/acetonitrile (30/70; Thermo Fisher Scientific Inc., USA) at a flow rate of 1 mL/min. The column temperature was 25 $^\circ\text{C}$. The detection wavelength was 254 nm. The final formulations were characterized by elemental analysis recorded on a Vario EL III elemental, and results were shown in Supporting Information Table S4.

The synthesis and characterization of compounds are shown in the Supporting Information.

4.4. In vitro studies

4.4.1. Receptor binding studies^{47–49}

The following specific radioligands and tissue sources were used: (a) the dopamine D₂ receptor [^3H] *N*-methylspiperone, from hD₂-CHO cells, (b) the dopaminergic D₃ receptor [^3H] *N*-methylspiperone, from hD₃-CHO cells, (c) the serotonin 5-HT_{1A} receptor [^3H] 8-OH-DPAT, from h5-HT_{1A}-CHO cells, (d) the serotonin 5-HT_{1B} receptor [^3H] GR125743, from h5-HT_{1A}-CHO cells, (e) the serotonin 5-HT_{2A} receptor [^3H] ketanserin in the presence of 4-piperidone hydrochloride hydrate (35 nmol/L), from h5-HT_{2A}-CHO cells, (f) the serotonin 5-HT_{2C} receptor [^3H] mesulergine, in the presence of spiperone (40 nmol/L), from rat cerebral cortex, (g) the serotonin 5-HT₆ receptor [^3H] lysergic acid diethylamide, from h5-HT₆-CHO cells, (h) the dopamine transporter (DAT) [^3H] WIN35428, from rat striatum, (i) the noradrenaline transporter (NET) [^3H] nisoxetine, from hNET-CHO cells (j) the serotonin transporter (SERT) [^3H] paroxetine, from hSERT-CHO cells (k) the histamine H₁ Receptor (H₁) [^3H] mepyramine, from guinea pig cerebellum, and (l) the adrenergic α 1 Receptor (α 1) [^3H] prazosin, from rat cerebral cortex.

The radioligand competitive binding assay for each receptor was performed as follows. Compound **23j** was dissolved in 50% (*v/v*) DMSO, and the compound concentration was 2×10^{-3} mol/L; dilution to the initial concentration of the new compound, 2×10^{-4} mol/L, contained 5% DMSO. For one receptor binding assays, total binding (TB) was determined in the presence of the radioligand. Nonspecific binding (NB) was determined in the presence of the radioligand and competitive ligand for the related

receptor, whereas compound binding (CB) was determined in the presence of the radioligand and compound **23j**. Each specific binding (SB) was calculated as the total binding (TB) minus the nonspecific binding (NB) at a particular concentration of radioligand. Each percentage of inhibition (%) was calculated as Eq. (1):

$$\text{Percentage of inhibition (\%)} = [(TB - CB)/(TB - NB)] \times 100 \quad (1)$$

Blank binding experiments contained 0.25% (*v/v*) DMSO were performed; DMSO had no effect. All compounds were tested at least three times over a 6-fold concentration range (10^{-5} to 10^{-10} mol/L). IC₅₀ values were determined by nonlinear regression analysis with fitting to the Hill equation curve. *K_i* values were calculated using the Cheng and Prussoff equation as Eq. (2):

$$K_i = IC_{50}/(1 + C/K_d) \quad (2)$$

where *C* represents the concentration of the hot ligand used and *K_d* is the receptor dissociation constant of each labeled ligand. The *K_i* value was derived from at least three independent experiments.

4.4.2. Total ERK1/2 and pERK1/2 measurement^{69,70}

Total ERK1/2 and pERK1/2 measurement was performed by using total ERK cellular kit (#64NRKPEG, Cisbio, Codolet, France) and advanced ERK phospho-T202/Y204 kit (#64AERPEG, Cisbio, Codolet, France). All steps were carried out per manufacturer instructions. In brief, CHO-D₂R cells or CHO-D₃R cells were grown at 37 $^\circ\text{C}$, 5% CO₂ in DMEM +10% FBS until approximately 80% confluent. Cells were seeded in polystyrene-treated 96-well cell culture plates at approximately 50,000 cells/well and cultured overnight in 50 μL serum-free growth media. After 18–24 h of overnight culture, tested compounds were prepared in DMEM+0.1% FBS, added to the cells and incubated at 37 $^\circ\text{C}$, 5% CO₂, for 15 min. For the measure of the antagonism, dopamine was added to the wells in 20 $\mu\text{mol/L}$ for p-ERK assessments and incubated at 37 $^\circ\text{C}$, 5% CO₂ for 7–8 min after the incubation of tested compounds. For the measure of the agonism, DMEM+0.1% FBS was added instead. Then, the supernatant was removed, and cells were lysed with $1 \times$ lysis buffer (prepared per manufacturer's protocol) for 30 min at room temperature (RT) while shaking. Next, 16 μL of cell lysates were transferred to an assay plate (384-OptiPlate, PerkinElmer). p-ERK antibodies were prepared and added per manufacturer's protocol: 2 μL of Eu³⁺ Cryptate working antibody (donor) solution and 2 μL of d2 working antibody (acceptor) solution were added to each well and incubated overnight at RT. Fluorescence emission at 2 different wave-lengths (665 and 620 nm) were measured on an Envision plate reader (PerkinElmer, Waltham, Massachusetts), and the HTRF ratio of the acceptor and donor emission signals for each well was calculated as Eq. (3):

$$\text{HTRF ratio} = (665 \text{ nm}/620 \text{ nm}) \times 10,000 \quad (3)$$

All samples were tested in duplicates. The results were calculated as a percent of control after dividing the phospho-ERK1/2 by total-ERK1/2. Data for each group were averaged and presented as mean \pm SEM. Data were assessed for normality (Shapiro–Wilk) and homoscedasticity (Brown–Forsythe). Statistical significance was determined by one-way analysis of variance

(ANOVA) with Tukey's multiple comparison post-test. Comparisons were considered statistically significant when $P < 0.05$.

4.4.3. hERG affinity

CHO cells were stably transfected with hERG cDNA and cultured in F12 medium (Gibco) supplemented with 10% (v/v) fetal bovine serum (FBS) and 0.5 mg/mL Geneticin (Invitrogen) at 37 °C in a humidified environment (5% CO₂/95% air). The cells were seeded out two days before reaching 70% confluency. Prior to use, the cells were washed in PBS and incubated with 5 mL Detachin (Genlantis) for 4–5 min at 37 °C to detach cells from the culture dish. The harvested cells were re-suspended in F12 medium at a density of 2 million cells/mL. The cells were transferred to a QPatch instrument (Sophion Bioscience, Denmark) and allowed to recover for 20 min in the Qstir cell preparation station on the Qpatch-8 before experiment. The tail currents of hERG channel were evaluated using the Q-patch automated patch clamp platform (Sophion Bioscience, Denmark). The following solutions were used during patch-clamp recording (compositions in mmol/L): internal solution: KCl 120, CaCl₂ 5.374, MgCl₂ 1.75, KOH 31.25, EGTA 10, HEPES 10, Na₂ATP 4, pH 7.2 (KOH); external solution: NaCl 145, KCl 4, MgCl₂ 1, CaCl₂ 2, HEPES 10, glucose 10, pH 7.4 (NaOH). All solutions were sterile filtered. Cells were clamped at –80 mV and hyperpolarized to –100 mV to monitor the change of series resistance. The voltage protocol for hERG ion channel started with a short (200 ms) –50 mV step to establish the baseline region. A depolarizing step was applied to the test potential of 20 mV for 2 s, and then the cell was depolarized to –50 mV to evoke outward tail currents. Currents were filtered using the internal Bessel filter in Qpatch. Recording started in external solution. After this control period, 5 increasing concentrations of the test compounds were applied, each for approximately 4 min to record a complete concentration–response curve. The last control period (saline) is used as baseline for data normalization. Cisapride (2 μmol/L) was applied as a reference inhibitor at the end of protocol. The sampling frequency is 2000 Hz. Data were acquired and analyzed using the PatchMaster software (HEKA). The compounds **23j**, **36a**, **36b** and **36f** were dissolved in extracellular solution to get different concentrations of solutions: 0.412, 1.23, 3.70, 11.1, 33.3, 100 μmol/L.

4.4.4. Cytotoxicity test

Cytotoxicity of selected compounds was determined using the cell counting kit-8 (CCK8) assay kit (Beyotime, Shanghai, China). Briefly, HEK293T, BV2, and PC12 were cultured in 96-well plates at a density of 8000 cells per well at 37 °C overnight. Then, different concentrations of selected compounds were added into cells and incubated for 24 h. According to the manufacture's instruction, 10 μL of CCK8 detection reagent was added into 100 μL of medium per well. After 1 h, absorbance was read at 450 nm for CCK8 using Spark[®] Multimode Microplate Reader. Cell inhibition was calculated as relative absorbance compared to a DMSO-only control. And dose–effect relationship curves were calculated for the IC₅₀.

4.5. In vivo efficacy studies

4.5.1. Animals and compounds

Male adult C57BL/6 mice (6–8 weeks old) and ICR mice (6–8 weeks old) were obtained from Beijing Vital River Lab Animal Technology Co., Ltd. All animals were housed in cages under artificial lighting from 7:00 AM to 7:00 PM, with free access to

food and water. Animals were assigned to different experimental groups randomly, each kept in a separate cage. All experimental procedures were approved by the Peking University Institutional Animal Care and Use Committee. All compounds used for *in vivo* assays were produced as the formation of hydrochloride with the superior water solubility, and the final formulations were characterized by elemental analysis (Table S5).

4.5.2. Catalepsy test^{32,49}

Mice were injected intraperitoneally with vehicle, RPD of 0.6, 1.2, 2.4, 4.8, 9.6 mg/kg, compound **23j** of 15, 30, 60, 120, 240 mg/kg, **36a/b/f** of 30, 60, 120, 240, 480 mg/kg. Catalepsy was tested individually 15, 30 and 45 min after injection. The test consisted in positioning the animal with its forepaws on the wood particle (3 cm in height) and recording how long it remained hanging onto the bar; the end point was 60 s and an all-or-none criterion was used. A mean immobility score of 30 s was used as the criterion for the presence of catalepsy. The number of the mice with positive reaction in each group was recorded. The ED₅₀, minimum effective doses (MED), and maximal effects (percent of cataleptic animals) were accordingly calculated.

4.5.3. Spontaneous locomotor test^{47,49}

ICR mice (10 mice in each group) were dosed with the vehicle and selected compounds (30 mg/kg) by intraperitoneal injection. Animals were placed in Plexiglas cages for evaluating locomotor activity. After the environmental adaptation for 30 min, the total locomotor distance of each animal was recorded for 15 min and automatically measured by the spontaneous activity video analysis system. All cages were changed after every test.

4.5.4. MK-801-induced hyperactivity^{47–49}

ICR mice (divided into several groups, 10 mice in each group) were intraperitoneally injected with vehicle (vehicle group and MK group) or increasing doses of selected compounds (3, 10, 30 mg/kg). RPD and CRP were used as the positive drug with the dose of 0.1, 0.3, 1, 3 mg/kg. After 10 min, were intraperitoneally injected with normal saline, while other groups of mice were challenged with 0.3 mg/kg of MK-801 s.c. After injection, mice were immediately placed in Plexiglas cages for evaluating locomotor activity for 60 min. The total locomotor distance of the mice movement during 60 min was automatically recorded and measured by the spontaneous activity video analysis system. All cages were changed after every test.

4.5.5. Apomorphine-induced climbing^{47–49}

ICR mice were divided into several groups with 10 mice in each group. The vehicle group and APO group of mice were intraperitoneally injected with vehicle. The tested compounds groups were intraperitoneally injected with increasing doses of compound **23j** and **36b** (0.3, 1, 3, 10, 30 mg/kg). After 30 min, the model group and tested groups were challenged with 1.0 mg/kg of the apomorphine in 0.9% NaCl +0.1% ascorbic acid by subcutaneous injection. After the injection of apomorphine, the mice immediately were placed in cylindrical wire cages (12 cm in diameter, 14 cm in height), and observed for climbing behavior at 10, 20, 30 min post dose. The climbing behavior was scored as follows: 4 paws on the cage floor with normal activity = 0 score; 4 paws on the cage floor with an increase in activity or sniffing = 1; 2 paws on the reseau occasionally = 2; 4 paws on the reseau occasionally = 3; 4 paws on the reseau all

the time = 4. RPD was used as the positive drug with the dose of 0.1, 0.3, 1, 3, 10 mg/kg.

4.5.6. Tail suspension test⁷¹

ICR mice (10 mice in each group) were orally dosed with vehicle, duloxetine (15 mg/kg) or increasing doses of **36b** (3, 10, 30 mg/kg) for 3 days. After the last administration for 30 min, the mice were suspended individually by the tail using adhesive tape (attached 2 cm from the tip of the tail) to a hook attached to a strain gauge and the behavior changes in 6 min of the mice were recorded by a camera system. Then, the latency time (the immobility first observed) was calculated and duration of immobility in the last 4 min of the recorded time was measured.

4.5.7. Forced swimming test⁷¹

ICR mice (10 mice in each group) were orally dosed with vehicle, duloxetine (15 mg/kg) or increasing doses of **36b** (3, 10, 30 mg/kg) for 3 days. After the last administration for 30 min, each mouse was placed in a clear cylindrical tank (40 cm tall × 20 cm diameter), filled with water (30 cm tall) at 24 ± 2 °C. Mice were judged as immobile when they float motionlessly. Mice were forced to swim freely for 6 min with record by a camera system, and then the latency time (the immobility first observed) was calculated. Then, the duration of immobility in the last 4 min was measured when analyzing. Water was changed after every test.

4.5.8. Novel object recognition training and testing⁴⁹

The first day of the experiment is the adaptation period. The mice were put into the empty box from the center of the side. The mice were allowed to adapt to the environment for 10 min freely. The second day is learning phase. Two object A were put into the box, 10 cm close to the same side of the box, and the distance between the two objects is 40 cm. Then the mice were put individually into the box and given 5 min explore the area and objects. Memory retention was tested 1.5 h after training. One of the two object A was replaced by an object B, then put the mice individually into the box and gave them 5 min to explore. The motion trails of the mice were recorded by the image processing system of computer. The NDI was calculated by Eq. (4):

$$\text{NDI (\%)} = (\text{Novel object interaction time} / \text{Total interaction time}) \times 100 \quad (4)$$

Mice were divided into 6 groups, 10 mice in each group. 5 groups of mice were orally dosed with vehicle, RPD (1 mg/kg) or increasing doses of compound **36b** (3, 10, 30 mg/kg) for 5 days, starting from 4 days before the adaption period. On the 5th day, the untreated group of mice and those dosed with RPD or compound **36b** were administrated i.p. with MK-801 (0.2 mg/kg) 30 min before the experiment.

4.5.9. Weight gain and serum prolactin

Mice (10 mice in each group) were orally dosed with vehicle, **23j** (30 mg/kg) or **36b** (30 mg/kg) for 28 days. The weight of each mouse was recorded before intragastric administration every day. The mice were killed by decapitation 180 min after the last treatment. Blood samples (2 mL) were collected and centrifuged (300×g for 30 min), and the serum prolactin of the resulting serum sample was determined by an ELISA kit from Elabscience cto.

4.6. In vivo metabolism studies

4.6.1. Pharmacokinetics study in mice⁷¹

The HPLC conditions were as follows: column, Diamonsil C18 (150 mm × 4.6 mm, 5 μmol/L, 120 Å); mobile phase, 0.1% formic acid in water/acetonitrile (Merck Company, Germany) (v/v, 0–8.0 min, 40:60); flow rate, 0.2 mL/min; column temperature, 40 °C. UV detection, 254 nm. ICR mice (*n* = 3/group) were dosed with compounds **23j/36b** via the tail vein for i.v. administration (3 mg/kg) or *p.o.* administration (10 mg/kg). After the last administration, 80 μL of orbital blood was extracted at 0.25, 0.5, 1, 2, 3, 4, 5, 6, 8 and 24 h. After separated by centrifugation (rpm = 18,000, 10 min), the plasma sample (30 μL) was prepared for high-pressure liquid chromatography/tandem mass spectrometry (LC–MS/MS) analysis by protein precipitation with acetonitrile (100 μL). The plasma samples were analyzed for drug and internal standard via an API 4000 Q trap mass spectrometer (Applied Biosystems, Foster City, CA, USA) coupled with a 1200 series HPLC system (Agilent, Santa Clara, CA, USA). Isocratic elution was used with 80% acetonitrile and 20% water with 0.1% formic acid to separate analytes. The total run time was 3 min, and the flow rate was 0.3 mL/min.

4.6.2. BBB penetration study in mice

At 0.5 and 2 h after the last administration, after euthanizing the mice using CO₂ gas, the blood was collected from the heart immediately and the plasma was treated the same way as above. The remaining blood was washed out from the circulation by performing cardiac perfusion with physiological saline containing 10 U/mL heparin. The brain was then removed from the skull and added to three volumes of PBS buffer per weight, homogenized, and stored at –20 °C. The compound concentrations in plasma and brain samples were determined via the LC–MS/MS protocol.

4.7. Statistical analysis

All values are presented as mean ± SEM or mean ± SD. For the calculation of EC₅₀, the variable slope model was used with Eq. (5):

$$Y = Y_{\min} + (Y_{\max} - Y_{\min}) / (1 + 10^{(\log EC_{50} - X) \times \text{HillSlope}}) \quad (5)$$

Differences between groups were analyzed by two-tailed Student's *t* test. One-way ANOVA followed by *post hoc* Bonferroni's or Donnet's multiple comparisons was used to compare more than two groups. Two-way ANOVA followed by *post hoc* Bonferroni's multiple comparisons test was used for comparison of a series of data collection among groups.

Acknowledgments

This research was supported by The National Key R&D Program (2022YFC2303700, China), the Ningxia Hui Autonomous Region Key Research and Development Project (2022BEG02042, China), the National Natural Science Foundation of China (82030108, 81803351), Open Fund of State Key Laboratory of Pharmaceutical Biotechnology, Nanjing University (KF-202304, China), the China Postdoctoral Science Foundation (2018M641122, China), and the National Major Scientific and Technological Special Project for Significant New Drugs Development (2018ZX09711002-013-004, 2018ZX09735-001, China).

Author contributions

Zhongtang Li devised the project and conceived the main conceptual ideas. Zhongtang Li and Fan Fang designed the compounds. Zhongtang Li and Fan Fang synthesized, purified, and characterized all compounds. Yiyang Li and Xuehui Lv performed receptors binding and functional study. Ruqiu Zheng and Peili Jiao characterized the selectivity study and hERG inhibitor. Guiwang Zhu and Zefang Jin carried out docking and modeling studies. Yuxi Wang, Xiangqing Xu and Yinli Qiu performed all *in vivo* experiments. The manuscript was written through contributions of all authors. Guisen Zhang, Zhongjun Li and Zhenming Liu revised and submitted the manuscript on behalf of other authors. Liangren Zhang provided the financial support for this project. All authors have given approval to the final version of the manuscript.

Conflicts of interest

The authors have no conflicts of interest to declare.

Appendix A. Supporting information

Supporting data to this article can be found online at <https://doi.org/10.1016/j.apsb.2023.07.024>.

References

- Lagerstrom MC, Schiöth HB. Structural diversity of G protein-coupled receptors and significance for drug discovery. *Nat Rev Drug Discov* 2008;**7**:339–57.
- Hauser AS, Attwood MM, Rask-Andersen M, Schiöth HB, Gloriam DE. Trends in GPCR drug discovery: new agents, targets and indications. *Nat Rev Drug Discov* 2017;**16**:829–42.
- Lutjens R, Rocher JP. Recent advances in drug discovery of GPCR allosteric modulators for neurodegenerative disorders. *Curr Opin Pharmacol* 2017;**32**:91–5.
- Beaulieu JM, Espinoza S, Gainetdinov RR. Dopamine receptors—IUPHAR review 13. *Br J Pharmacol* 2015;**172**:1–23.
- Sokoloff P, Giros B, Martres MP, Bouthenet ML, Schwartz JC. Molecular cloning and characterization of a novel dopamine receptor (D₃) as a target for neuroleptics. *Nature* 1990;**347**:146–51.
- Searle G, Beaver JD, Comley RA, Bani M, Tziortzi A, Slifstein M, et al. Imaging dopamine D₃ receptors in the human brain with positron emission tomography, [¹¹C]PHNO, and a selective D₃ receptor antagonist. *Biol Psychiatr* 2010;**68**:392–9.
- Cho DI, Zheng M, Kim KM. Current perspectives on the selective regulation of dopamine D(2) and D(3) receptors. *Arch Pharm Res (Seoul)* 2010;**33**:1521–38.
- Jönsson EG, Flyckt L, Burgert E, Crocq M-A, Forslund K, Mattila-Evenden M, et al. Dopamine D₃ receptor gene Ser9Gly variant and schizophrenia: association study and meta-analysis. *Psychiatr Genet* 2003;**13**:1–12.
- Shonberg J, Herenbrink CK, Lopez L, Christopoulos A, Scammells PJ, Capuano B, et al. A structure-activity analysis of biased agonism at the dopamine D₂ receptor. *J Med Chem* 2013;**56**:9199–221.
- Orsolini L, De Berardis D, Volpe U. Up-to-date expert opinion on the safety of recently developed antipsychotics. *Expert Opin Drug Saf* 2020;**19**:981–98.
- Stemp G, Ashmeade T, Branch CL, Hadley MS, Hunter AJ, Johnson CN, et al. Design and synthesis of *trans*-N-[4-[2-(6-cyano-1,2,3,4-tetrahydroisoquinolin-2-yl)ethyl]cyclohexyl]-4-quinolinecarboxamide (SB-277011): a potent and selective dopamine D(3) receptor antagonist with high oral bioavailability and CNS penetration in the rat. *J Med Chem* 2000;**43**:1878–85.
- Kumar V, Bonifazi A, Ellenberger MP, Keck TM, Pommier E, Rais R, et al. Highly selective dopamine D₃ receptor (D₃R) antagonists and partial agonists based on eticlopride and the D₃R crystal structure: new leads for opioid dependence treatment. *J Med Chem* 2016;**59**:7634–50.
- Micheli F, Bacchi A, Braggio S, Castelletti L, Cavallini P, Cavanni P, et al. 1,2,4-Triazolyl 5-Azaspiro[2.4]heptanes: lead identification and early lead optimization of a new series of potent and selective dopamine D₃ receptor antagonists. *J Med Chem* 2016;**59**:8549–76.
- Chen J, Levant B, Jiang C, Keck TM, Newman AH, Wang S. Tranylcypromine substituted *cis*-hydroxycyclobutyl-naphthamides as potent and selective dopamine D(3) receptor antagonists. *J Med Chem* 2014;**57**:4962–8.
- Sun X, Gou HY, Li F, Lu GY, Song R, Yang RF, et al. Y-QA31, a novel dopamine D₃ receptor antagonist, exhibits antipsychotic-like properties in preclinical animal models of schizophrenia. *Acta Pharmacol Sin* 2016;**37**:322–33.
- Reilly SW, Riad AA, Hsieh CJ, Sahlholm K, Jacome DA, Griffin S, et al. Leveraging a low-affinity diazaspino orthosteric fragment to reduce dopamine D(3) receptor (D(3)R) ligand promiscuity across highly conserved aminergic G-protein-coupled receptors (GPCRs). *J Med Chem* 2019;**62**:5132–47.
- Micheli F, Bernardelli A, Bianchi F, Braggio S, Castelletti L, Cavallini P, et al. 1,2,4-Triazolyl octahydropyrrolo[2,3-*b*]pyrroles: a new series of potent and selective dopamine D₃ receptor antagonists. *Bioorg Med Chem* 2016;**24**:1619–36.
- Ananthan S, Saini SK, Zhou G, Hobrath JV, Padmalayam I, Zhai L, et al. Design, synthesis, and structure-activity relationship studies of a series of [4-(4-carboxamidobutyl)]-1-arylpiperazines: insights into structural features contributing to dopamine D₃ versus D₂ receptor subtype selectivity. *J Med Chem* 2014;**57**:7042–60.
- Diaz GJ, Daniell K, Leitza ST, Martin RL, Su Z, McDermott JS, et al. The [3H]dofetilide binding assay is a predictive screening tool for hERG blockade and proarrhythmia: comparison of intact cell and membrane preparations and effects of altering [K⁺]_o. *J Pharmacol Toxicol Methods* 2004;**50**:187–99.
- Moritz AE, Free RB, Weiner WS, Akano EO, Gandhi D, Abramyan A, et al. Discovery, optimization, and characterization of ML417: a novel and highly selective D(3) dopamine receptor agonist. *J Med Chem* 2020;**63**:5526–67.
- Das B, Vedachalam S, Luo D, Antonio T, Reith ME, Dutta AK. Development of a highly potent D₂/D₃ agonist and a partial agonist from structure-activity relationship study of *N*(6)-(2-(4-(1*H*-indol-5-yl)piperazin-1-yl)ethyl)-*N*(6)-propyl-4,5,6,7-tetrahydrobenzo[*d*]thiazole-2,6-diamine analogues: implication in the treatment of Parkinson's disease. *J Med Chem* 2015;**58**:9179–95.
- Newman AH, Grundt P, Cyriac G, Deschamps JR, Taylor M, Kumar R, et al. *N*-(4-(4-(2,3-Dichloro- or 2-methoxyphenyl)piperazin-1-yl)butyl)heterobiarylcarboxamides with functionalized linking chains as high affinity and enantioselective D₃ receptor antagonists. *J Med Chem* 2009;**52**:2559–70.
- Di Martino RMC, Cavalli A, Bottegoni G. Dopamine D₃ receptor ligands: a patent review (2014–2020). *Expert Opin Ther Pat* 2022;**32**:605–27.
- Millan MJ, Loiseau F, Dekeyne A, Gobert A, Flik G, Cremers TI, et al. S33138 (*N*-[4-[2-[(3*a*S,9*b*R)-8-cyano-1,3*a*,4,9*b*-tetrahydro[1]benzopyrano[3,4-*c*]pyrrol-2(3*H*)-yl]-ethyl]phenyl-acetamide], a preferential dopamine D₃ versus D₂ receptor antagonist and potential antipsychotic agent: III. Actions in models of therapeutic activity and induction of side effects. *J Pharmacol Exp Therapeut* 2008;**324**:1212–26.
- Millan MJ, Mannoury la Cour C, Novi F, Maggio R, Audinot V, Newman-Tancredi A, et al. S33138 [*N*-[4-[2-[(3*a*S,9*b*R)-8-cyano-1,3*a*,4,9*b*-tetrahydro[1]-benzopyrano[3,4-*c*]pyrrol-2(3*H*)-yl]-ethyl]phenylacetamide], a preferential dopamine D₃ versus D₂ receptor antagonist and potential antipsychotic agent: I. Receptor-binding profile and functional actions at G-protein-coupled receptors. *J Pharmacol Exp Therapeut* 2008;**324**:587–99.

26. Redden L, Rendenbach-Mueller B, Abi-Saab WM, Katz DA, Goenjian A, Robieson WZ, et al. A double-blind, randomized, placebo-controlled study of the dopamine D3 receptor antagonist ABT-925 in patients with acute schizophrenia. *J Clin Psychopharmacol* 2011;**31**:221–5.
27. Bhatena A, Wang Y, Kraft JB, Idler KB, Abel SJ, Holley-Shanks RR, et al. Association of dopamine-related genetic loci to dopamine D3 receptor antagonist ABT-925 clinical response. *Transl Psychiatry* 2013;**3**: e245-e.
28. Micheli F, Arista L, Bertani B, Braggio S, Capelli AM, Cremonesi S, et al. Exploration of the amine terminus in a novel series of 1,2,4-triazolo-3-yl-azabicyclo[3.1.0]hexanes as selective dopamine D3 receptor antagonists. *J Med Chem* 2010;**53**:7129–39.
29. Nathan PJ, O'Neill BV, Mogg K, Bradley BP, Beaver J, Bani M, et al. The effects of the dopamine D(3) receptor antagonist GSK598809 on attentional bias to palatable food cues in overweight and obese subjects. *Int J Neuropsychopharmacol* 2012;**15**:149–61.
30. Appel NM, Li SH, Holmes TH, Acri JB. Dopamine D3 receptor antagonist (GSK598809) potentiates the hypertensive effects of cocaine in conscious, freely-moving dogs. *J Pharmacol Exp Therapeut* 2015;**354**:484–92.
31. Nielsen S, Gowing L, Sabioni P, Le Foll B. Pharmacotherapies for cannabis dependence. *Cochrane Database Syst Rev* 2019;**1**: CD008940.
32. Gyertyan I, Kiss B, Saghy K, Laszy J, Szabo G, Szabados T, et al. Cariprazine (RGH-188), a potent D3/D2 dopamine receptor partial agonist, binds to dopamine D3 receptors *in vivo* and shows antipsychotic-like and procognitive effects in rodents. *Neurochem Int* 2011;**59**:925–35.
33. Slifstein M, Abi-Dargham A, Girgis RR, Suckow RF, Cooper TB, Divgi CR, et al. Binding of the D3-preferring antipsychotic candidate F17464 to dopamine D3 and D2 receptors: a PET study in healthy subjects with [(11)C]-(+)-PHNO. *Psychopharmacology (Berl)* 2020;**237**:519–27.
34. Bitter I, Lieberman JA, Gaudoux F, Sokoloff P, Groc M, Chavda R, et al. Randomized, double-blind, placebo-controlled study of F17464, a preferential D(3) antagonist, in the treatment of acute exacerbation of schizophrenia. *Neuropsychopharmacology* 2019;**44**:1917–24.
35. Cosi C, Martel JC, Auclair AL, Collo G, Cavalleri L, Heusler P, et al. Pharmacology profile of F17464, a dopamine D(3) receptor preferential antagonist. *Eur J Pharmacol* 2021;**890**:173635.
36. Chien EY, Liu W, Zhao Q, Katritch V, Han GW, Hanson MA, et al. Structure of the human dopamine D3 receptor in complex with a D2/D3 selective antagonist. *Science* 2010;**330**:1091–5.
37. Bonifazi A, Yano H, Ellenberger MP, Muller L, Kumar V, Zou MF, et al. Novel bivalent ligands based on the sumanirole pharmacophore reveal dopamine D2 receptor (D2R) biased agonism. *J Med Chem* 2017;**60**:2890–907.
38. Kumar V, Moritz AE, Keck TM, Bonifazi A, Ellenberger MP, Sibley CD, et al. Synthesis and pharmacological characterization of novel *trans*-cyclopropylmethyl-linked bivalent ligands that exhibit selectivity and allosteric pharmacology at the dopamine D3 receptor (D3R). *J Med Chem* 2017;**60**:1478–94.
39. Newman AH, Battiti FO, Bonifazi A. 2016 Philip S. Portuguese medicinal chemistry lectureship: designing bivalent or bitopic molecules for G-protein coupled receptors. The whole is greater than the sum of its parts. *J Med Chem* 2020;**63**:1779–97.
40. Perez-Nueno VI, Ritchie DW, Rabal O, Pascual R, Borrell JI, Teixido J. Comparison of ligand-based and receptor-based virtual screening of HIV entry inhibitors for the CXCR4 and CCR5 receptors using 3D ligand shape matching and ligand-receptor docking. *J Chem Inf Model* 2008;**48**:509–33.
41. Chen WL, Wang ZH, Feng TT, Li DD, Wang CH, Xu XL, et al. Discovery, design and synthesis of 6*H*-anthra[1,9-*cd*]isoxazol-6-one scaffold as G9a inhibitor through a combination of shape-based virtual screening and structure-based molecular modification. *Bioorg Med Chem* 2016;**24**:6102–8.
42. Sato T, Yuki H, Takaya D, Sasaki S, Tanaka A, Honma T. Application of support vector machine to three-dimensional shape-based virtual screening using comprehensive three-dimensional molecular shape overlay with known inhibitors. *J Chem Inf Model* 2012;**52**:1015–26.
43. Baell JB, Holloway GA. New substructure filters for removal of pan assay interference compounds (PAINS) from screening libraries and for their exclusion in bioassays. *J Med Chem* 2010;**53**:2719–40.
44. Rankovic Z. CNS physicochemical property space shaped by a diverse set of molecules with experimentally determined exposure in the mouse brain. *J Med Chem* 2017;**60**:5943–54.
45. Wang S, Dong G, Sheng C. Structural simplification: an efficient strategy in lead optimization. *Acta Pharm Sin B* 2019;**9**:880–901.
46. Dou X, Huang H, Li Y, Jiang L, Wang Y, Jin H, et al. Multistage screening reveals 3-substituted indolin-2-one derivatives as novel and isoform-selective c-Jun N-terminal kinase 3 (JNK3) inhibitors: implications to drug discovery for potential treatment of neurodegenerative diseases. *J Med Chem* 2019;**62**:6645–64.
47. Chen Y, Wang S, Xu X, Liu X, Yu M, Zhao S, et al. Synthesis and biological investigation of coumarin piperazine (piperidine) derivatives as potential multireceptor atypical antipsychotics. *J Med Chem* 2013;**56**:4671–90.
48. Cao X, Chen Y, Zhang Y, Qiu Y, Yu M, Xu X, et al. Synthesis and biological evaluation of new 6-hydroxypyridazinone benzisoxazoles: potential multi-receptor-targeting atypical antipsychotics. *Eur J Med Chem* 2016;**124**:713–28.
49. Cao X, Zhang Y, Chen Y, Qiu Y, Yu M, Xu X, et al. Synthesis and biological evaluation of fused tricyclic heterocycle piperazine (piperidine) derivatives as potential multireceptor atypical antipsychotics. *J Med Chem* 2018;**61**:10017–39.
50. Xu P, Huang S, Mao C, Krumm BE, Zhou XE, Tan Y, et al. Structures of the human dopamine D3 receptor-G(i) complexes. *Mol Cell* 2021;**81**:1147–11459. e4.
51. Recanatini M, Poluzzi E, Masetti M, Cavalli A, De Ponti F. QT prolongation through hERG K(+) channel blockade: current knowledge and strategies for the early prediction during drug development. *Med Res Rev* 2005;**25**:133–66.
52. Raschi E, Ceccarini L, De Ponti F, Recanatini M. hERG-related drug toxicity and models for predicting hERG liability and QT prolongation. *Expert Opin Drug Metabol Toxicol* 2009;**5**:1005–21.
53. Li M. Antipsychotic-induced sensitization and tolerance: behavioral characteristics, developmental impacts, and neurobiological mechanisms. *J Psychopharmacol* 2016;**30**:749–70.
54. Kiss B, Horvath A, Nemethy Z, Schmidt E, Laszlovszky I, Bugovics G, et al. Cariprazine (RGH-188), a dopamine D(3) receptor-preferring, D(3)/D(2) dopamine receptor antagonist-partial agonist antipsychotic candidate: *in vitro* and neurochemical profile. *J Pharmacol Exp Therapeut* 2010;**333**:328–40.
55. Wang Y, Gao J, Zhao S, Song Y, Huang H, Zhu G, et al. Discovery of 4-arylthiophene-3-carboxylic acid as inhibitor of ANO1 and its effect as analgesic agent. *Acta Pharm Sin B* 2021;**11**:1947–64.
56. Marchese G, Casu G, Casti P, Spada GP, Pani L. Evaluation of amphetamine-induced hyperlocomotion and catalepsy following long-acting risperidone administration in rats. *Eur J Pharmacol* 2009;**620**:36–41.
57. Winship IR, Dursun SM, Baker GB, Balista PA, Kandratavicius L, Maia-de-Oliveira JP, et al. An overview of animal models related to schizophrenia. *Can J Psychiatr* 2019;**64**:5–17.
58. McCutcheon RA, Reis Marques T, Howes OD. Schizophrenia—an overview. *JAMA Psychiatr* 2020;**77**:201–10.
59. Jones CA, Watson DJ, Fone KC. Animal models of schizophrenia. *Br J Pharmacol* 2011;**164**:1162–94.
60. Porsolt RD, Castagne V, Hayes E, Virley D. Nonhuman primates: translational models for predicting antipsychotic-induced movement disorders. *J Pharmacol Exp Therapeut* 2013;**347**:542–6.
61. Campiani G, Butini S, Fattorusso C, Catalanotti B, Gemma S, Nacci V, et al. Pyrrolo[1,3]benzothiazepine-based serotonin and dopamine receptor antagonists. Molecular modeling, further structure–activity

- relationship studies, and identification of novel atypical antipsychotic agents. *J Med Chem* 2004;**47**:143–57.
62. Krynicki CR, Upthegrove R, Deakin JFW, Barnes TRE. The relationship between negative symptoms and depression in schizophrenia: a systematic review. *Acta Psychiatr Scand* 2018;**137**:380–90.
63. Noda Y, Yamada K, Furukawa H, Nabeshima T. Enhancement of immobility in a forced swimming test by subacute or repeated treatment with phencyclidine: a new model of schizophrenia. *Br J Pharmacol* 1995;**116**:2531–7.
64. Arauchi R, Hashioka S, Tsuchie K, Miyaoka T, Tsumori T, Limoa E, et al. Gunn rats with glial activation in the hippocampus show prolonged immobility time in the forced swimming test and tail suspension test. *Brain Behav* 2018;**8**:e01028.
65. Noda Y, Kamei H, Mamiya T, Furukawa H, Nabeshima T. Repeated phencyclidine treatment induces negative symptom-like behavior in forced swimming test in mice: imbalance of prefrontal serotonergic and dopaminergic functions. *Neuropsychopharmacology* 2000;**23**:375–87.
66. Young ME, Sutherland S. The spatiotemporal distinctiveness of direct causation. *Psychon Bull Rev* 2009;**16**:729–35.
67. Grayson B, Idris NF, Neill JC. Atypical antipsychotics attenuate a sub-chronic PCP-induced cognitive deficit in the novel object recognition task in the rat. *Behav Brain Res* 2007;**184**:31–8.
68. Lomize MA, Lomize AL, Pogozheva ID, Mosberg HI. OPM: orientations of proteins in membranes database. *Bioinformatics* 2006;**22**:623–5.
69. Brule C, Perzo N, Joubert JE, Sainsily X, Leduc R, Castel H, et al. Biased signaling regulates the pleiotropic effects of the urotensin II receptor to modulate its cellular behaviors. *Faseb J* 2014;**28**:5148–62.
70. Ayoub MA, Trebaux J, Vallaghe J, Charrier-Savourmin F, Al-Hosaini K, Gonzalez Moya A, et al. Homogeneous time-resolved fluorescence-based assay to monitor extracellular signal-regulated kinase signaling in a high-throughput format. *Front Endocrinol* 2014;**5**:94.
71. Li Z, Cai G, Fang F, Li W, Fan M, Lian J, et al. Discovery of novel and potent *N*-methyl-D-aspartate receptor positive allosteric modulators with antidepressant-like activity in rodent models. *J Med Chem* 2021;**64**:5551–76.